White Matter Microstructural Correlates of Cognitive and Motor Functioning Revealed via Multimodal Multivariate Analysis

Multivariate Multimodal analysis Associations Reveal Differential Patterns

Alasmar, Z.[1,2], Tremblay, S. A.[2,3,4], Baumeister T. R.[5,6,7], Carbonell F.[8], Iturria-Medina, Y.[5,6,7], Gauthier C. J.[3,4], Steele C. J.[1,2,9]

1 Psychology Dept., Concordia University
2 School of Health, Concordia University
3 EPIC Centre, Montreal Heart Institute
4 Department of Physics, Concordia University
5 Ludmer Center for NeuroInformatics and Mental Health,
6 McConnell Brain Imaging Center, Montreal Neurological Institute and Hospital
7 Neurology and Neurosurgery Department, McGill University,
8 Biospective Inc.
9 Neurology, Max Planck Institute for Human Cognitive and Brain Sciences

1. Abstract

Recent advances in cognitive neuroscience emphasise the importance of healthy white matter (WM) in optimal behavioural functioning. It is now widely accepted that brain connectivity via WM contributes to the emergence of behaviour. However, the association between the microstructure of WM fibres and behaviour is poorly understood. This is in part due to indirect and overlapping methods of assessing microstructure, and the use of overly simplistic approaches in assessing behaviour. Here, we used the Mahalanobis Distance (D2) to integrate 10 metrics of WM derived from multimodal neuroimaging that have strong ties to microstructure. The D2 metric was chosen because it accounts for metrics' covariance as it measures the voxelwise distance between every subject and the average; thus providing a robust multiparametric assessment of microstructure. To examine WM-behaviour associations, we used multivariate correlation to examine the voxelwise correlates of 2 cognitive and 2 motor tasks, which allowed us to compare within and across domains in WM. We observed that behaviour is organised in cognitive, motor, and integrative variables that are widespread in their associations with WM, from frontal to parietal regions. Our results highlight the complex nature of microstructure and behaviour, and show the need for multivariate modelling when examining brain-behaviour associations.

2. Introduction

Recent advances in neuroimaging techniques have allowed researchers to non-invasively assess brain structure and function in health and disease (Calhoun, 2018; Tardif et al., 2016). These techniques have become crucial in understanding the neural underpinnings of cognitive and motor behaviour. Though most research has focused on brain function, it is now increasingly clear that function is supported by the connectivity and microstructure of white matter (WM) (Thiebaut de Schotten et al., 2020; Thiebaut de Schotten & Forkel, 2022). WM can be assessed with diffusion weighted magnetic resonance imaging (dMRI), providing both an estimation of grey matter connectivity patterns and a quantification of different components of WM microstructure (Duval et al., 2017; Soares et al., 2013). Importantly, there are many quantitative dMRI-derived metrics that are differentially sensitive to different aspects of microstructure (e.g. organisation, myelination, and density), thereby serving as a rich multivariate source of individual microstructural differences that can be directly related to behaviour. Investigating how WM microstructure is related to normative behaviour is crucial for enhancing our basic understanding of brain function and a first step in investigating how pathological change affects structure and behaviour and may be ameliorated by targeted treatment (Thiebaut de Schotten & Forkel, 2022).

WM is composed of axons that vary in their myelination, density, and overall composition (Mezer et al., 2013; Stikov et al., 2015). Changes in healthy WM are largely due to refinements in the signal conduction environment (Hagmann et al., 2010) to support optimal function (Pajevic et al., 2014), resulting in observable behavioural effects such as enhanced/reduced performance. Myelination is known to shape this environment by fine tuning signal conduction (Knowles et al., 2022), with animal models providing key evidence for myelin remodulation during motor learning and cognition (e.g. in memory; McKenzie et al., 2014; Pan et al., 2020). While there is a huge body of work in human imaging focused on cortical function and structure, there has been much less work to explore how the microstructure of the underlying WM connections support behaviour. Expanding from initial cross-sectional human work (e.g., Bengtsson et al., 2005; Johansen-Berg et al., 2007), neuroplastic changes in non-invasive dMRI-derived measures of WM have been shown to be associated with a wide range of behaviours, including motor skills (Scholz et al., 2009; Steele et al., 2013; Taubert et al., 2010; Tremblay et al., 2021) memory (de Lange et al., 2017), and normative motor development

(Muetzel et al., 2008). Thus, individual differences in WM microstructure that arise as a function of individual experience can be assessed with non-invasive MRI and used to probe the relationship with behaviour in both healthy and disease states. Previous research has largely relied on assessing individual contrasts with univariate approaches (most commonly assessing fractional anisotropy [FA] and mean diffusivity [MD]), which problematically assumes independence when MRI metrics have overlapping characteristics that cannot be directly tied to a single microstructural or physiological source (Raghavan et al., 2021; Tardif et al., 2016). In contrast, each metric can be considered within a multivariate framework as indirect measures that provide overlapping complementary information for a more comprehensive characterization of WM microstructure (Tremblay et al., 2024).

dMRI-derived metrics provide measurements of WM microstructure such as myelination and fibre characteristics (Raffelt et al., 2017; Raghavan et al., 2021; Tardif et al., 2016). Simple and complex diffusion models can be computed from dMRI multi-shell high angular resolution protocols, such as the diffusion tensor (DTI; Soares et al., 2013), fibre orientation distribution function (ODF; Tournier et al., 2019), and neurite orientation dispersion and density imaging (NODDI; Zhang et al., 2012). It is therefore possible to extract measures assessing microstructural tissue properties via these models including myelin integrity, fibre thickness, and intracellular volumes. While the metrics derived from DTI, FOD, and NODDI have been unquestionably useful in human neuroscience and often interpreted as specific physiological parameters, there is no clear one-to-one metric-parameter mapping. Further, we and others have shown that there is a high degree of correlation between metrics within and across models (Carter et al., 2022; Figley et al., 2022; Tremblay et al., 2024; Uddin et al., 2019). This suggests that strong conclusions based on theoretical interpretation of a single metric are often difficult to justify.

Human behaviour is typically measured with specific tasks, such as item recall, that are individually interpreted as an assessment of a specific domain (e.g., working memory). However, reducing complex behaviours to a singular interpretation ignores how the connected brain supports the many interacting systems that lead to behaviour (Varoquaux & Poldrack, 2019). Tasks can be considered as imperfect assessments of the multiple brain systems that support them, with differential and partially overlapping weighting depending on the specific task (e.g., reading and motor tasks both recruit the visual system to different extents). Standard univariate

approaches to understanding the brain-behaviour relationship implicitly ignore both the overlap between tasks and with brain systems (Poldrack, 2010; Varoquaux et al., 2018). Multivariate approaches have shown promise in identifying latent behavioural factors (Schöttner et al., 2023) that may be more directly tied to brain structure and function (Price & Friston, 2005; Varoquaux et al., 2018), with recent work illustrating the power of the approach in identifying multiple functional and/or structural regions supporting memory and visually guided motor function (Pur et al., 2022), and cognition (Voigt et al., 2023; Ziegler et al., 2013).

While most human neuroimaging studies have tended to focus on GM, studies examining WM have been increasing in number. However, most of these studies assess microstructure via univariate analyses of metrics with overlapping contributions of tissue properties (Tardif et al., 2016). The non-specific nature of the metrics makes it difficult to disentangle the contribution of tissue properties to the imaging modalities, and give rise to shared and overlapping changes in the MR signal. To help overcome this problem, we recently developed an integrative quantitative assessment of WM microstructure using multimodal neuroimaging (Tremblay et al., 2024). We proposed that combining neuroimaging metrics that are highly correlated and represent overlapping physiological tissue properties tie intimately to the underlying microstructure. This is achieved by integrating multiple metrics, while accounting for the covariance between them, in a single multivariate score. We developed *mvComp*, a toolbox to compute voxelwise Mahalanobis Distance (D2). D2 is a generalisation of the euclidean distance that measures the distance between a point and a distribution in a multi-dimensional space (Mahalanobis, 1936). It also explicitly incorporates the covariance between features so as to not bias the distance with collinearity. D2 has already been used in a number of human MRI studies to assess microstructural deviation as a severity marker in traumatic brain injury (Taylor et al., 2020), relate epilepsy duration to alterations in WM tract FA (Owen et al., 2021), and quantify individual microstructural variation to drive clustering in the corpus callosum (Tremblay et al., 2024).

In the present study, we aimed to identify the unique and overlapping spatial patterns of the relationship between white matter microstructure and cognitive and motor behaviour. We used the D2 to integrate MRI metrics while accounting for their shared covariance and performed a partial least squares (PLS) multivariate statistical analysis to relate multivariate behaviour on four cognitive and motor tasks to voxel-wise white matter D2. We hypothesised

that integrating multiple measures of microstructure and behaviour together yields more biologically interpretable and meaningful brain-behaviour associations, and that there will be differential patterns in D2's relationship to behaviour across WM.

3. Method

a. Participants

For this investigation, we used data from the WU-Minn Human connectome project (HCP S1200 release). The HCP is a large cohort of healthy young adults with MRI, DWI, and behavioural measures spanning cognition and motor functioning. The full procedure is described in depth elsewhere (Van Essen et al., 2013). Briefly, our sample consisted of 1065 healthy young adults (age: M: 28.76 years, SD: 3.68, 556 females), with no history of psychiatric, neurological, or neuropsychological disorders, and no history of substance abuse. We excluded participants with incomplete imaging data and/or invalid acquisitions.

b. Multimodal Neuroimaging Protocols

All imaging was conducted by the HCP on a custom 3T Connectome Skyra MRI scanner with a 32-channel head coil. Anatomical scans were acquired in the first session, and included T1-weighted as well as T2-weighted protocols (Van Essen et al., 2013). The T1w scans were acquired using a 3D-MPRAGE sequence while a 3D T2-SPACE sequence was used for T2w. Anatomical scans were acquired with a 0.7mm isotropic resolution (FOV=224x224). T1w had a TI=1000, TE=2.14, and TR=2400, while T2w TE was 565 and TR of 3200. The DWI acquisition was conducted during the fourth session. DWI data (TE/TR=89.5/5520 ms, FOV=210×180 mm) were multi-shell with b-values of 1000, 2000 and 3000 s/mm^2 and a 1.25 mm isotropic resolution, 90 uniformly distributed directions, and 6 b=0 volumes. More details on the acquisitions can be found at: https://www.humanconnectome.org/hcp-protocols-ya-3t-imaging. The imaging data of 1065 young healthy adults, those who had undergone T1w, T2w and diffusion-weighted imaging, were preprocessed. The data of 64 participants were excluded in the current study due to poor cerebellar coverage.

c. Microstructural features from multimodal neuroimaging

Neuroimaging preprocessing

All MRI scans were preprocessed following the minimal preprocessing procedure by the HCP (Glasser et al., 2013). The HCP preprocessing procedure included intensity normalisation of b=0 scans along with corrections for eddy current and susceptibility-induced distortions using the different phase encoding directions. It also included co-registration of DWI to native T1w

with a rigid body transformation on the mean b=0 scans, which was also applied to realign all diffusion directions (Bvecs) as well. Finally, motion and gradient nonlinearity correction were applied. All subsequent data preprocessing steps as well as neuroimaging metric extraction are described in detail in Tremblay and colleagues (2024) and described briefly below.

First, the preprocessed multishell diffusion data was bias-field corrected using the ANTs' N4 algorithm via *dwibiascorrect* from MRtrix3 (Tustison et al., 2010). Using MRtrix3's *dwi2tensor* (Tournier et al., 2019), we calculated the diffusion tensor and extracted its metrics with *tensor2metric*, which yielded voxelwise fractional anisotropy (FA), mean diffusivity (MD), axial diffusivity (AD), and radial diffusivity (RD). DTI metrics maps were transformed into the group template space as described below. We then used the multi-tissue Constrained Spherical Deconvolution (CSD) to estimate a WM fibre response function, and later WM fibre composition. We first segmented all tissue types (WM, GM, CSF) by applying FSL's *5ttgen* (via the MRtrix3 wrapper, Smith et al., 2012; Tournier et al., 2019) on T1w scans. We computed the response function of each tissue type for all participants from the minimally preprocessed DWI data (without bias field correction) and the five-tissue-type (5tt) image using the *msmt_5tt* algorithm of the *dwi2response* function (Dhollander et al., 2016, 2018; Jeurissen et al., 2014; D. A. Raffelt et al., 2017). The response function represents the diffusion profile of a specific fibre population and is used to estimate the Orientation Distribution Functions (ODFs) with CSD. The WM, GM and CSF response functions were then averaged across all participants, resulting in a single response function for each of the three tissue types. Multi-shell multi-tissue CSD was then performed in each individual with the average response functions to obtain an estimation of orientation distribution functions (ODFs) for each tissue type (Jeurissen et al., 2014). This step is performed using the *dwi2fod msmt_csd* function of MRtrix3 within a brain mask. Bias field correction and global intensity normalisation, which normalises signal amplitudes to make subjects comparable, were then performed on the ODFs, using the *mtnormalise* function in MRtrix3 (Dhollander et al., 2016, 2018; Jeurissen et al., 2014; D. A. Raffelt et al., 2017).

Group space coregistration

While most registration approaches are focused on optimising GM alignment, between different subjects and across modalities, we opted to perform a WM-focused registration. For this, we used a multi-contrast registration that was primarily driven by WM FODs but also

included information about grey matter and CSF. We created population templates for WM, GM, and CSF FODs based on a subset of 200 participants using MRtrix3's *population_template* function, with the following parameters: nl_update_smooth= 1.0, nl_disp_smooth= 0.75 to apply a gaussian smoothing on the gradient and displacement field, respectively. We subsequently computed the warps between all subjects and our population template using MRtrix3's *mrregister* function with identical regularisation parameters. These warps were subsequently applied to the brain masks extracted by using Brain Extraction Tool (*BET*) on T1w, WM FODs, DTI metrics (FA, MD, AD, and RD), T1-weighted (T1w), and T2-weighted (T2w) images through *mrtransform* (Raffelt et al., 2012). During this step, the WM FODs were transformed without reorientation, aligning the image voxels but not the "fibre bundle elements" (fixels; Raffelt et al., 2015). To create a template mask encompassing only the voxels with data from all subjects, we computed the intersection of all warped brain masks using the *mrmath* min function. Additionally, we warped the WM probability images from the five-tissue-type (5tt) segmentation to the group template space in order to generate a WM mask, and computed the group average probability of WM at each voxel. Lastly, we generated an FOD template average and retained the T1w and T2w images in their native resolution (0.7mm) and calculated the T1w/T2w ratio to generate a proxy myelin map, which was then warped to the FOD template (Glasser & Van Essen, 2011).

The FOD template was then segmented to extract the WM fixel mask. This fixel mask determines the fibre bundle elements (fixels) within each voxel. Fixel segmentation is then performed on the WM FODs of each subject. The fixels are aligned with the template using subject-to-template warps (*fixelreorient* function) and mapped to the corresponding fixels in the fixel mask (*fixelcorrespondence* function). This ensures a consistent set of fixel directions for all subjects. We computed 2 fixel metrics in addition to the computation of the apparent fibre density (FD) of each fixel. First, the fibre bundle cross-section (FC) metric was computed to measure the expansion or contraction required for the fibre bundle to fit the fixel template, and the fibre density and cross-section (FDC) metric was calculated by multiplying the FD and FC metrics, representing the overall capacity of a fibre bundle to carry information.

To incorporate all metrics into a unified multi-modal model, the fixel metric maps were summarised into voxelwise maps. Instead of deriving the measure of total fibre density (FDtotal) per voxel from fibre-specific FD, we used the sum of FOD lobe integrals. This summation

yielded more reproducible estimates, as demonstrated in previous studies (Calamante et al., 2015). For the fibre cross-section voxel aggregate measure, we computed the weighted mean of FC using the *fixel2voxel* function's mean option. This measure represents the average expansion or contraction required to align fibre bundles within a voxel to the fixels in the template. The weighting factor was based on FD (fibre density), ensuring that bundles with higher density exerted a greater influence on the voxelwise FC value compared to those with lower density. Finally, to assess the overall information-carrying capacity at each voxel, we computed the voxelwise sum of FDC (fibre density and cross-section) using the *fixel2voxel* function's sum option. This measure represents the cumulative capacity to carry information within a voxel (Raffelt et al., 2017).

The bias field-corrected DWI data was also fit with the neurite orientation dispersion and density imaging (NODDI) model using the python implementation of Accelerated Microstructure Imaging via Convex Optimization (AMICO) (Daducci et al., 2015; Zhang et al., 2012). Initially, small variations in b values were addressed by assigning the nearest target b value (0, 1000, 2000, or 3000) to each value in the b-values file. This step aimed to prevent the fitting algorithm from considering slightly different b values as distinct diffusion shells, given that the b-values from the HCP exhibit slight variations. Subsequently, a diffusion gradient scheme file was created based on the b-vectors and the modified b-values file. The response functions were computed for all compartments, and the fitting procedure was performed on the unbiased DWI volumes, specifically within the brain mask excluding non-brain voxels. The resulting parameters obtained from the fitting process were the intracellular volume fraction (ICVF) assessing neurite density (i.e. interpreted as axonal density in WM) and orientation dispersion index (OD) assessing the extent of dispersion around the mean orientation (Zhang et al., 2012).

In total, 10 voxelwise microstructural measures were computed for each of the 1001 subjects to use as features in our analyses. These features were 4 DTI measures (FA, MD, RD, AD), 3 ODF measures (FC, FD, FDC), and 2 NODDI measures (ICVF & OD) and T1w/T2w. We then computed voxelwise averages for each of these features and the covariance between each pair of features across all of WM voxels.

d. Multivariate distance model

We computed the Mahalanobis Distance (D2), a voxelwise multivariate distance, to incorporate all 10 microstructural features while accounting for the covariance between them. Due to the high covariance between imaging features that capture shared and overlapping biological and physiological mechanisms (Raghavan et al., 2021; Tardif et al., 2016), accounting for it in an explicit statistical model is a more precise way to intimately tie derived metrics to microstructure (Tremblay et al., 2024). The voxelwise approach permits group-level analysis since it results in individual subject D2 maps that are direct assessments of the multivariate differences from the average microstructure. To avoid biassing the average with each subject's data when distances between the subject and the average is computed, a leave-one-subject-out approach was implemented. Here, each subject was removed from the calculated metric averages when that subject's voxelwise D2 map was computed.

The distance between each subject's microstructural features (i.e., the 10 features) and the average of those features at a given voxel is calculated, resulting in a subject distance vector of the shape 10x1. Then, the distance vector is divided by the covariance between features (in our mvComp approach, this is achieved by multiplication with the pseudoinverse of the covariance matrix; see Tremblay et al., 2024). The same procedure is conducted for each voxel in every subject, resulting in voxelwise D2 maps for each of them.

e. Detecting outliers

We computed D2 for all 1001 subjects in our sample. Due to the large number of voxels and features used per subject, outliers were observed in these individualised D2 maps. Therefore, we removed every participant with extensive voxelwise outliers, based on a threshold of 5 standard deviations from their average D2 value. That is, if a participant's D2 map contained 55 or more voxels with D2 values larger than 5 SD (i.e. > 0.07% voxels) of their own voxelwise average, that participant was dropped from the analysis. This value was chosen as the optimal tradeoff between outlier removal and retaining a large sample - further increasing the cutoff results in an ~50% drop in sample size. As D2 is computed relative to the average, we reran the D2 computations on the resulting final smaller sample of 735 subjects. We then applied a power transformation at each voxel (across all subjects) to normalise the D2 distribution and z-scored for standardisation. Lastly, standardised D2 z-scores with probabilities

that exceeded 99.7% in each tail of the distribution were transformed to the closest value on a per-voxel basis since they were not deemed as outliers but rather large values (i.e. values larger than ~3SD were transformed to 3SD).

f. Behavioural tasks

We used 4 tasks to assess cognition and motor functioning from the NIH toolbox, which were included with the HCP (Reuben et al., 2013; Weintraub et al., 2013). To assess motor functioning, we used the Grip Strength task (GST) and the 9-Hole Pegboard task (9-HPT), examining strength and dexterity respectively. In the GST, subjects were asked to squeeze a hand dynamometer as hard as they can, while in the 9-HPT, they are timed as they place 9 pegs in holes on a board and then remove them as quickly as possible. The tasks chosen to assess cognition were the card sorting task (CST) and the list sorting task (LST), both well validated and standardised tasks widely used in examining cognitive flexibility and working memory respectively. All behavioural measures were also power-transformed and z-scored. The voxelwise correlations between these tasks and D2 are shown in supplementary figure 1.

g. Age and sex correction

To account for the potentially confounding effects of age and sex on neuroimaging metrics (Weber et al., 2022), each of the behavioural data as well as the voxelwise D2 values were fitted with a robust linear regression (task ~ age + sex, D2 ~ age + sex) and the residuals retained for subsequent analysis to statistically remove their effects. As with the imaging data, age and sex measures were power-transformed and z-scored prior to inclusion in the analyses.

h. Statistical analyses

A multivariate partial least squares-singular value decomposition (PLS-SVD) analysis was used to examine the association between D2 and the 4 behavioural measures (GST, 9-HPT, CST, and LST). This approach applies a singular value decomposition (SVD) to the brain-behaviour covariance matrix to extract latent variables (LV) (McIntosh & Mišić, 2013). Given a matrix M of voxel and task associations, SVD decomposes M into USV^T, such that U has the shape (voxel x LV), whereas V^T is an (LV x task) matrix. Decomposing the covariance matrix allows for the extraction of latent variables that have the largest amount of explained brain-behaviour covariance, along with the weight (importance) of each task and voxel on each latent variable. The weight of each voxel is represented by the columns of U, while the weight

of each task is represented by the row of V^T. Statistical significance of the LVs was assessed with a 1000 permutation of the PLS-SVD decomposition. In other words, we conducted 1000 PLS-SVD iterations, shuffling the behavioural input each time and extracting the explained covariance from each iteration. After extracting all the explained covariance values from each iteration, those that were larger in the original decomposition than the shuffled iterations were deemed statistically significant. We conducted 1000 bootstrap iterations for each voxel and task of every latent variable to assess statistical significance of that voxel or task (by bootstrapping the U and V^T matrices). For each bootstrapping iteration, behavioural as well as D2 data were resampled with replacement, and for each resampled set the PLS-SVD decomposition was rerun. This allows the calculation of confidence intervals around each task/voxel weight. For permutation and bootstrap testing, the significance level was set to a family-wise error corrected $p < 0.05$. The outcomes from this analysis were the brain-behaviour explained covariance, behavioural and microstructural (i.e. D2) PLS scores for each subject, and task and voxel weights for each LV.

Significant findings were further assessed to identify their WM structural connectivity profiles using a normative model of whole-brain connectivity. For each significant LV, we chose a maximum of 3 regions of spatially connected voxels with large weights in order to individually identify the set of streamlines passing through them. This approach is identical to that used in identifying the network effects of brain lesions (Karnath et al., 2018; Talozzi et al., 2023; Thiebaut de Schotten et al., 2020; Zayed et al., 2020). Here, we used a previously constructed streamline connectivity model that consisted of 10 million representative streamlines between all GM regions in our template space. After extracting the streamlines passing through the clusters, the GM connectivity profile of the WM passing through these clusters was summarised using the Automated anatomical labelling atlas 3 (AAL; Rolls et al., 2015) and using the *tck2connectome* function of MRTrix3 (Tournier et al., 2019).

mvComp was used to compute voxelwise D2 scores for each subject, and in-house pipelines to perform all data correction on D2 and behavioural data. We used MATLAB to run the PLS-SVD analysis as well the permutation and bootstrapping iterations.

4. Results

We used D2 and PLS-SVD to examine the multivariate relationship between microstructure and cognitive and motor behaviour. We found that the first 3 latent variables extracted via PLS-SVD were statistically significant, and explained 39.01%, 25.23%, and 19.04% of brain-behaviour covariance, respectively (fig. 1). The PLS scores of D2 and behaviour were positively correlated in all LVs (r=0.39, r=0.69, r=0.70 for LV1, LV2 and LV3, respectively; panel a in fig 2,3,4). LV1 was characterised by positive behavioural weights on both cognitive tasks (cognitive flexibility and working memory) and one motor task (manual dexterity) (fig. 2b). Significant voxels, distributed in WM underlying frontal and parietal regions, as well as cerebellar WM, had mostly negative weights, indicating negative brain-behaviour associations (fig. 2c). In the second LV, grip strength showed a strong positive association and cognitive flexibility weighed less heavily, while WM voxels associated with this pattern had positive and negative values in parietal and cerebellar WM (fig. 3b,c). Lastly, LV3 showed negative weights of working memory while manual dexterity weighed positively (fig. 4b). There were strong negative and positive weights in adjacent regions underlying frontal WM as well as in the corpus callosum (fig. 4c). Results for each LV are discussed in the next sections.

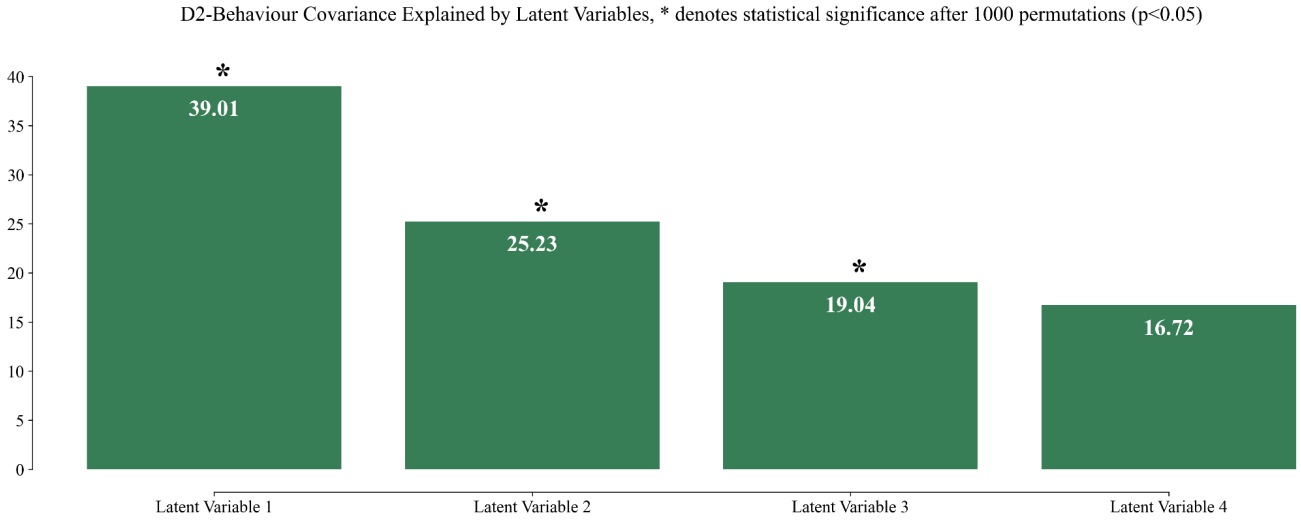

Figure 1: The amount of explained brain-behaviour covariance per latent variable. * denotes statistically significant after 1000 permutations (FWE $p < 0.05$).

a. Latent Variable 1

The first LV revealed a moderate association between transformed D2 and behavioural scores ($r = 0.39$, $p < 0.001$; fig. 2a). We found that cognitive flexibility, working memory, and manual dexterity were statistically significant in their positive weights on LV1 (fig. 2b). WM voxels adjacent to frontal, temporal, and cerebellar regions had negative weights, while parietal regions were either negatively weighted (e.g. corticospinal tract) or positively weighted (only in WM underlying the pericentral sulcal regions), as shown in fig. 2c. Put differently, these distributed negative voxels across the WM along with the positively weighted tasks are negatively correlated given their opposite signs, while the positively weighted voxels are positively correlated with behaviour.

To examine the connectivity profile of largest voxel weights that are spatially connected, we extracted 3 clusters situated in WM underlying the left pericentral sulcus and left prefrontal WM, and in the right corticospinal tract. The connectivity profile of each is shown in fig. 2e. We observed that for the first cluster in fig. 2d, the largest proportion of connections passed through the left supplementary motor area (left SMA), followed by the right SMA. The prefrontal WM cluster was found to connect the left putamen, for which the largest proportion of connections led to, followed by the left frontal inferior orbital cortex. Lastly, streamlines passing through the corticospinal tract cluster connected the right thalamus (largest proportion of connections), followed by the right parietal cortices, then the right precuneus are maximally connected through it.

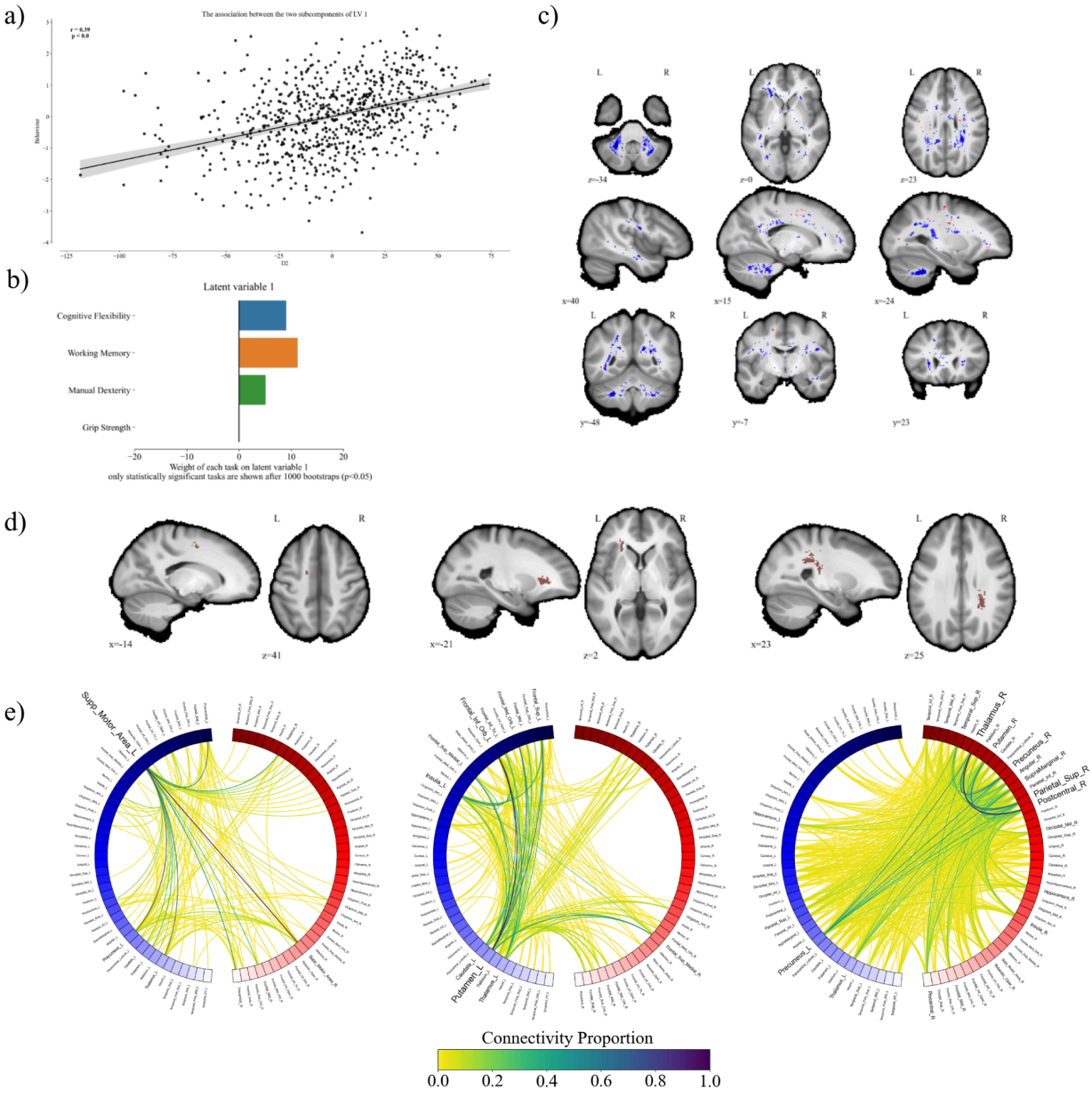

Figure 2: Decomposition results of the first latent variable. (a) PLS score correlation, (b) weights of statistically significant tasks, (c) weights of statistically significant voxels, (d) identified clusters of interest, (e) connectivity profile of clusters based on AAL.

b. Latent Variable 2

The second LV revealed a stronger association between PLS scores (D2 and tasks; $r = 0.69$, $p<0.05$; fig. 3a). Two tasks were positively weighted on this LV; cognitive flexibility and grip strength, while. However, manual dexterity had a negative weight. This LV was predominantly weighted by grip strength, while working memory weight was not statistically significant after 1000 bootstraps (fig. 3b). Unlike LV1, there were positively- and negatively-weighted voxels distributed in WM (fig. 3c). The positively weighted voxels were in the left parietal, right prefrontal, right temporal, and right superior cerebellar WM, whereas negatively weighted voxels were scattered in left frontal, callosal, and inferior cerebellar WM. The positive voxels in parietal and frontal regions are maximally positively correlated with cognitive flexibility and grip strength, but they are negatively correlated to manual dexterity. On the other hand, the negative voxels in frontal and colossal WM are negatively associated with cognitive flexibility and grip strength, but positively associated with manual dexterity.

Again, to examine the connectivity profile of some of the statistically significant regions, we extracted 3 clusters situated in WM of the left corticospinal tract, genu of the corpus callosum, and WM underlying th in an k toe right primary mo. tor area (fig. 3d). Similarly to what was observed in LV1, the connectivity profile of the first cluster was dominated by left thalamic and parietal regions. The genu of the corpus callosum was the main hub of interhemispheric connectivity, mainly the frontal cortices (e.g. superior medial cortex) and left and right caudate nuclei. As expected, the streamlines passing through the cluster underlying WM of M1 largely affected the connectivity of M1, followed by the right thalamus and the putamen.

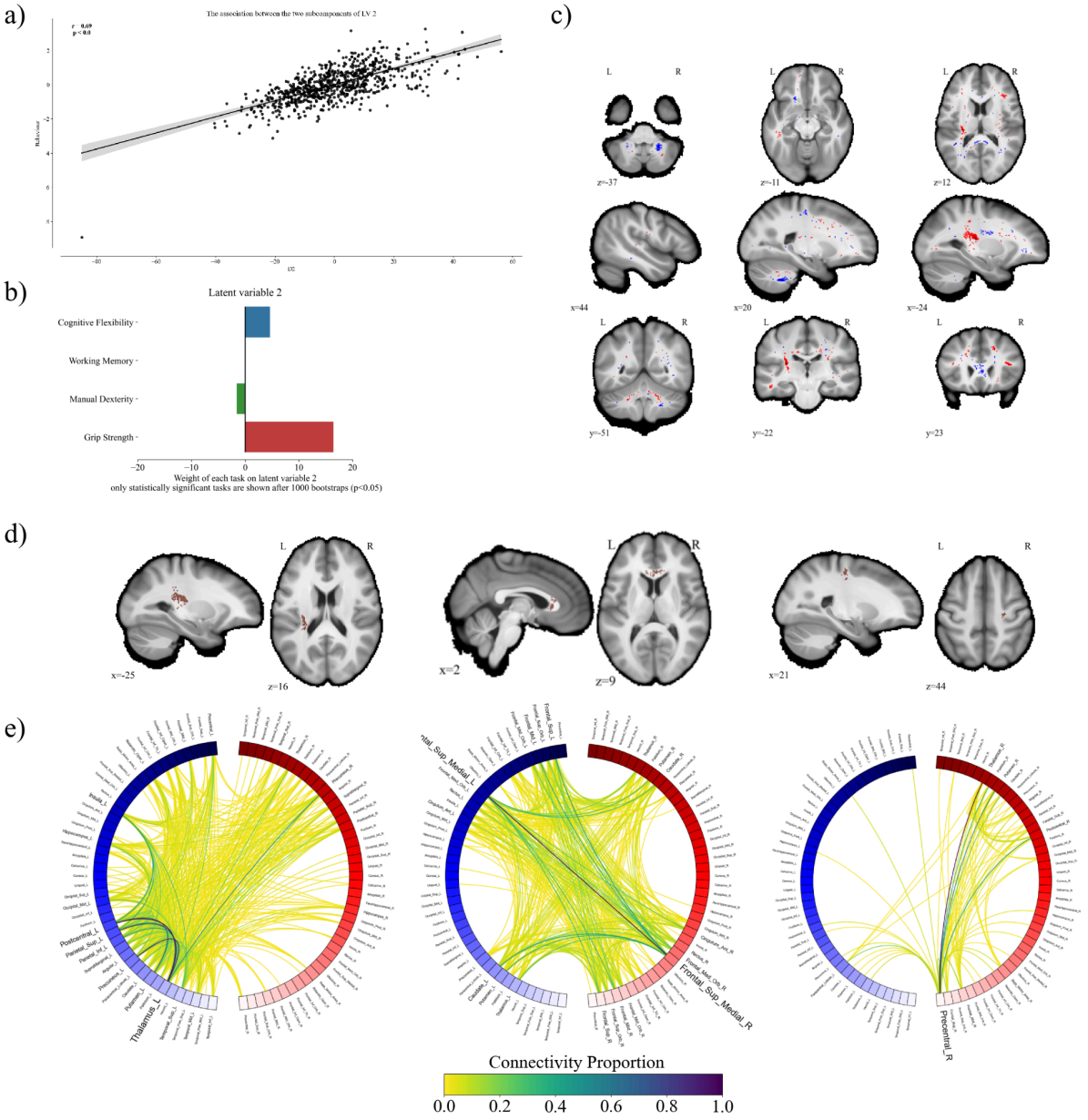

Figure 3: Decomposition results of the second latent variable. (a) PLS score correlation, (b) weights of statistically significant tasks, (c) weights of statistically significant voxels, (d) identified clusters of interest, (e) connectivity profile of clusters based on AAL.

c. Latent Variable 3

The third latent variable (LV) showed a similar correlation of transformed brain-behaviour scores to LV2, with a correlation coefficient of 0.70 ($p<0.05$; fig. 4a). Working memory and manual dexterity weighed heavily on this LV, albeit in opposite directions. Memory task was negatively weighted whereas dexterity weighed positively (fig. 4b). There were negatively and positively weighted voxels distributed in WM. Significant positive voxels were in prefrontal WM, adjacent to negative voxels. There were also positively weighted voxels in the right CST and in the splenium of the corpus callosum (fig. 4c). Manual dexterity was positively associated with the positive clusters in the left frontal, CST, and colossal WM while working memory was negatively associated with these regions, and vice versa. On the other hand,

We identified 3 clusters of statistically significant weights (fig. 4d), 2 of which were in prefrontal WM and one in the CST. The negative prefrontal cluster encompassed streamlines connecting the left frontal inferior orbital cortex. The adjacent positive cluster contained streamlines of the left frontal superior medial cortex. Lastly, the positive cluster in the CST was the passage of streamlines connecting the right precuneus, thalamus, and parietal cortices.

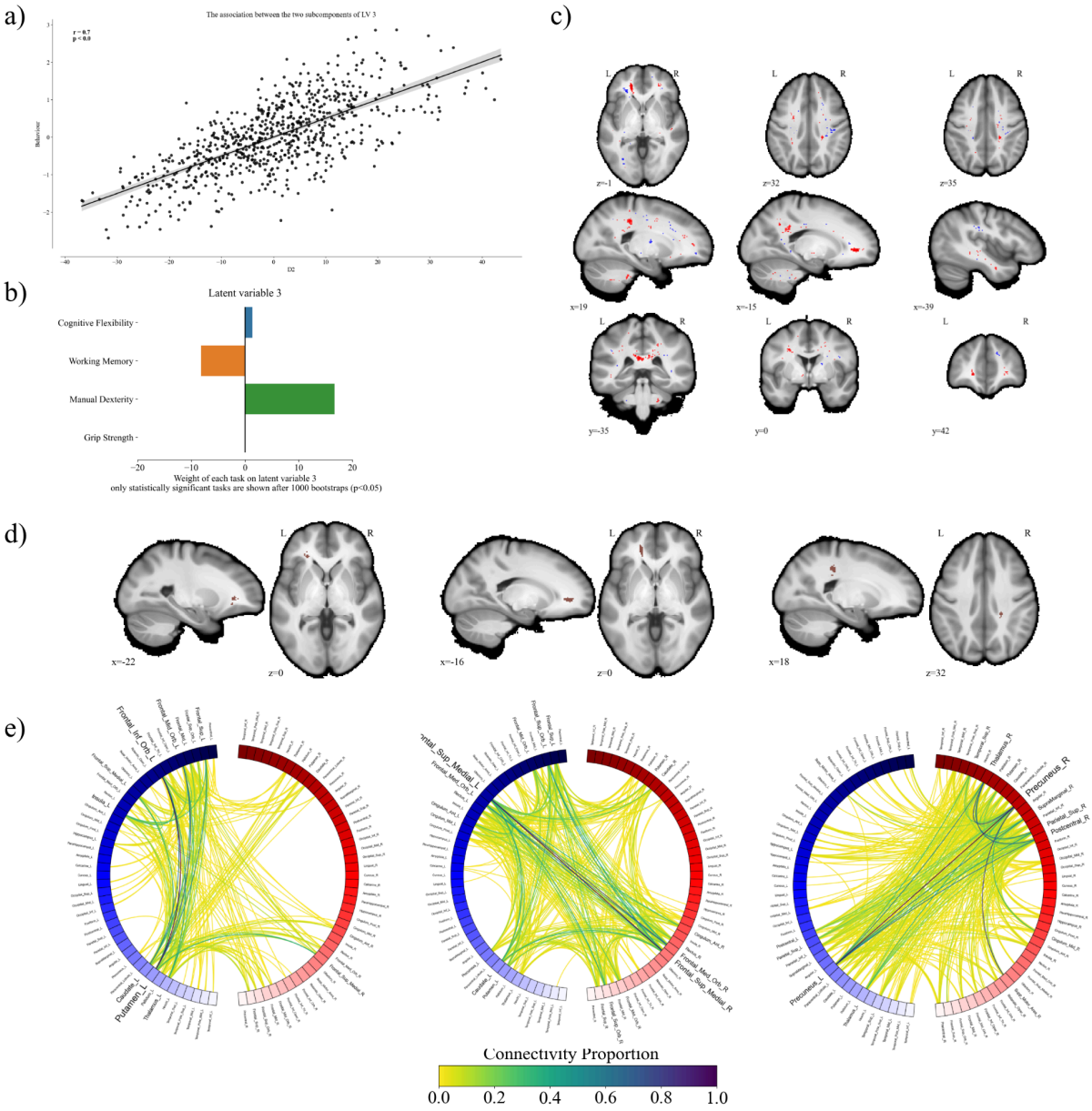

Figure 4: Decomposition results of the third latent variable. (a) PLS score correlation, (b) weights of statistically significant tasks, (c) weights of statistically significant voxels, (d) identified clusters of interest, (e) connectivity profile of clusters in d) based on AAL.

5. Discussion

The goal of the current study was to examine the association between white matter microstructure and behaviour using a multivariate analysis, incorporating 10 neuroimaging metrics and 4 behavioural tasks. By integrating these metrics, we were able to tie non-invasive neuroimaging to WM microstructure, and quantitatively compare across healthy cognitive and motor function. We used the mvComp toolbox to compute voxelwise D2 scores from neuroimaging metrics while accounting for their covariance. We then extracted latent variables of the spatial pattern of association between D2 and 4 tasks spanning motor and cognitive function. We sought to expand recent directives in neuroscience that emphasised the need for holistic mappings of behaviour on the brain (Varoquaux et al., 2018) to WM analysis. In order to do so, we used multivariate statistical integration of brain and behaviour which have shown enhanced validity and reliability compared to traditionally used techniques (Yoo et al., 2019). We extracted multidomain behavioural variables and found their WM microstructural correlates in a large sample of healthy young adults. We observed 3 statistically significant latent variables that explain a total of 83% of the brain-behaviour associations (fig. 1), and decompose behavioural functioning into higher order cognitive and premotor functioning (LV1; fig. 2), motor functioning (LV2; fig. 3), and integrative cognitive-motor functioning (LV3; fig. 4).

We used D2 to integrate dMRI-derived metrics which have been shown to be linked strongly to WM microstructure as described in Tremblay and colleagues (2024). There have been recent implementations which suggest that D2 is a more sensitive biomarker in epilepsy, traumatic brain injury, and in detecting individual variability in WM connectivity (Guerrero-Gonzalez et al., 2022; Owen et al., 2021; Taylor et al., 2020). However, our approach differs from these studies in a number of ways. First, rather than integrating multiple correlated neuroimaging metrics, these studies integrated the same measure across multiple WM tracts. This approach results in a single D2 score per participant, which could be used as a severity, classification, or prediction score at the expense of spatial information. That is, it is not possible to determine the location of differences within WM for each subject. On the contrary, our results show a whole WM differential pattern by using multiple microstructural metrics at the voxel level, which is both specific to the subject and the location within WM. Given the specificity of our approach, we also performed multivariate statistical analysis to investigate the association between voxelwise D2 scores and 4 behavioural tasks. We used partial least squares techniques,

which is increasing in popularity in neuroimaging research due to its robustness and sensitivity (McIntosh & Lobaugh, 2004; McIntosh & Mišić, 2013). This technique allowed us to provide a WM-behaviour mapping and explore the holistic nature of the relationship between microstructure and cognitive and motor functions that would not have been possible with univariate approaches.

First, the association between transformed scores of microstructure and behaviour were statistically significant for three of the four latent variables (panel a in fig. 2,3,4). The latent variables we identified provide a more comprehensive and holistic characterization of the relationships with behaviour than a univariate approach with each of the tasks separately (supplementary fig. 1). That is, combining multiple cognitive and motor tasks allowed us to extract the microstructural correlates of behaviour that are stronger and more holistic than univariate techniques. In all cases, we observed that better performance on cognitive (fig. 2a), motor (fig. 3a), and integrative (fig. 4a) behaviours, were correlated with greater distances (D2) in WMwhite matter microstructure. This is in agreement with the current frameworks in cognitive neuroscience that focus on the complex modelling of behaviour, starting with Price and Friston (2005), and more recently expanded on in Varoquaux and colleagues (2018) and Varoquaux and Poldrack (2019). These authors suggested that past and current neuroscientific evidence is overly reductionist, which limits its interpretability and generalizability across behavioural domains. Our method avoids oversimplifying behaviour, and rather extracts latent variables that ground behaviour in microstructure. Hence, it provides a path for the development of ontologies beyond the cortex and into WM. Overall, the effects we observed could be due to plastic changes in WM that lead to enhanced performance, or practice-induced changes in WM. Although it is not possible to assess which one precedes the other (Price & Friston, 2005), our technique shows that combining multiple measures of behaviour with multiple measures of microstructure is a stronger approach than independent univariate approaches.

Based on the behavioural weights of each latent variable, we showed that the first LV represented higher order cognitive and premotor skills, the second LV represented the motor behaviour, and the third LV represented integrative functioning (panel b, fig. 2,3,4). These findings emphasise the connectedness and interplay of different components of behaviour during a task (Schöttner et al., 2023). For instance, while cognitive tasks (i.e. cognitive flexibility and working memory) loaded strongly on LV1, the dexterity task weighed similarly on it. This is

likely due to the premotor execution functions required in the task, which are the planning of the reaching and grasping motions (fig. 2b). Dexterity has been previously grouped with cognition tasks via experimental manipulation, and when behavioural latent spaces were explored via machine learning (Rodríguez-Aranda et al., 2016; Schöttner et al., 2023). Previous studies examining the neural correlates of fine motor skills suggest that many cortical regions are involved in this complex task, including visuospatial and somatosensory areas (Sobinov & Bensmaia, 2021). This is contrasted with the second LV, where dexterity and grip strength weigh strongly, in addition to the cognitive flexibility task (fig. 3b). Of note here is that the working memory task is the only task that does not require the participants to use their arms to perform it (Weintraub et al., 2013). This was backed up by the lack of statistically significant weight of this task, and the positive weight of the cognitive flexibility of the card sorting task. Indeed, meta-analytical evidence from functional imaging during cognitive flexibility tasks shows activation in cognitive and motor areas of the cortex (Buchsbaum et al., 2005). Furthermore, we observed that tasks that require macro-level movement (i.e., gross movement) are dissociable from the fine motoric ones. This is supported by the positive weights of cognitive flexibility and grip strength, and the negative weight of dexterity (fig. 3b). Lastly, the third LV shows strong positive and negative weights of cognitive and motor tasks, reflecting the integrative nature of this variable. This integrative nature could only be extracted using multivariate techniques, and the use of multiple tasks spanning multiple behavioural domains. However, it does not match the clustering of Schöttner and colleagues (2023), which focuses on similarity between the loadings of behavioural tasks. One potential reason for this mismatch between our work and theirs is that our decomposition aims to extract latent brain-behavioural associations rather than behavioural associations alone. Thus the incorporation of WM microstructure in behavioural analysis provides a grounding for behaviour in neuroanatomy. There is evidence for disrupted cognitive-motor integration in TBI in relationship to cortical functioning (Sergio et al., 2020) and post-concussion temporal WM (Hurtubise et al., 2020). However, to our knowledge this is the first exploration of healthy integrative functioning in WM with such a multivariate approach. Therefore, in light of our findings, further research is required to assess the effects of incorporating WM microstructural with behavioural findings.

When examining the voxel weights, we observed widespread shared and overlapping patterns across WM in all LVs (panel c, fig. 2,3,4). These findings expand our understanding of

the complexity of brain-behaviour associations, emphasising the active role of WM microstructure in supporting higher-order cognitive processes, motor skills, and the integration of cognitive and motor functions. This is evident in the voxels' weights that span regions traditionally labelled regions as cognitive, motor, and higher-order integration. For instance, frontal and parietal regions for cognitive functions, parietal, cerebellar, and frontal for motor skills, and prefrontal WM for integrative functioning. An interesting pattern of voxel weights emerges between LVs. First, the cognitive LV (LV1) is mostly negatively distributed indicating that better performance on cognitive tasks is associated with smaller deviations of WM microstructure (i.e. larger D2). This pattern is observed for anterior and posterior frontal in addition to parietal WM. Our results are concordant with stroke disconnectome research, which shows cognitive and dexterous impairment with stroke-related disconnection in these regions (Talozzi et al., 2023). Moreover, cortical regions involved in premotor functions, visuospatial imagery, and executive skills are connected through these WM regions (Krüger et al., 2020; Sobinov & Bensmaia, 2021; Suchan et al., 2002). Namely, the left and right SMA, the left and right precuneus, and lastly the left putamen and frontal cortices, respectively. Therefore, it is possible that an interplay between microstructure and connectivity within WM gives rise to these behaviours. However, since our results come from a large sample of healthy individuals, we demonstrated that it is possible to localise cognitive functioning in WM prior to injury with only an individual differences approach. This could aid in symptom prediction and personalised treatment following tissue damage. Second, the motor LV is positively and negatively weighted differentially across all of WM. Unsurprisingly, the second LV's positive voxels are highly associated with motor function, and are distributed in WM underlying left motor regions. This effect is largely due to the recruitment of these regions in signal conduction, and the modulation of the microstructure for optimal motor performance (Sampaio-Baptista et al., 2013). The corticospinal tract was positively associated with gross motor performance, and negatively with fine motor skills. Here, all these tasks required motor execution, and a simple motor task such as grip strength had the largest weight. This is also supported by the cortices most connected through these clusters. For instance, we observed maximal connectivity of the left thalamus, left and right peri-central and frontal superior cortices in these clusters. For the third latent variable, integration of motor functioning with cognitive abilities have been shown to involve prefrontal and parietal WM as well as the splenium of the corpus callosum. These are consistent findings

linking motor, executive and working memory functioning to prefrontal areas (Thiebaut de Schotten & Forkel, 2022). Microstructural differences in these regions may be part of a larger network of cortical regions connected through WM, since the extracted cortical regions indicate that prefrontal GM is involved in integrative functioning (Seidler et al., 2012). Therefore, our observations in the prefrontal WM indicate a modulation of microstructure to support cortical functioning.

This study is not without limitations. We used 4 tasks spanning cognition and motor behaviours to provide a holistic brain-behaviour mapping. However, in order to provide a complete behavioural atlas grounded in WM microstructure, more tasks should be incorporated. Schöttner and colleagues (2023) show that using dimensionality reduction on a large battery of tasks, and extracting factors provided a good tradeoff between variance, reliability, and validity in behavioural assessments. Also, there are other functions, such as sensory and emotional functions, that are not for each of the measures we used that are not accounted for with these only 4 tasks, such as sensory and emotional behaviour (see Varoquaux & Poldrack, 2019). Therefore, future examinations should use similar dimensionality reduction techniques to Schöttner et al., (2023) while also incorporating emotion, language, and sensory measures. This will provide a more complete atlas of human behaviour, and disentangle the contribution of microstructural differences across WM to healthy functioning. Moreover, the Mahalanobis distance suffers from two main issues. First, it is a squared metric that does not distinguish the directionality of deviation from the average. Therefore, it is not possible using our method to assess whether there has been an increase or a decrease from the average in WM microstructure. The directionality could be an important factor in assessing longitudinal change, where the average is substituted as the baseline. Second, given that it is a distance to the average, voxelwise D2 values are arbitrary units of how different the microstructure is for a given subject. Guerrero-Gonzalez and colleagues (2022) applied the Wilk's criterion in order to define a statistical significance threshold for D2 scores (Penny, 1996), which would help in identifying the largest distance in a sample. However, given that D2 requires normality (Mahalanobis, 1936), computing a threshold of significance for this metric may be biassed in non-normal large samples. In future studies, permutation and reshuffling approaches may prove more beneficial in identifying robust and significant D2 values, while also identifying small deviations in order to

remove them. Future studies should also use longitudinal designs to explore within subject microstructural changes and their relationships to behaviour.

Conclusion

In conclusion, we provide a holistic mapping between cognitive and motor behaviours and white matter microstructure. We achieve this goal by using the Mahalanobis distance (D2) computed from 10 microstructural metrics, and decomposing the association between D2 and 4 behavioural measures assessing cognitive flexibility, working memory, dexterity and strength. We show that using multivariate statistical analysis provides stronger brain-behaviour associations and is able to extract latent variables of cognitive, motor and integrative function. We also provide spatial mappings between these 3 domains of behaviour and WM microstructure displayed as the strongest associations across WM. We extend our analysis to the cortical GM, and show that there exists an interplay between connectivity and microstructure in order to give rise to and sustain healthy human behavioural functioning.

6. References

Bengtsson, S. L., Nagy, Z., Nagy, Z., Nagy, Z., Nagy, Z., Skare, S., Forsman, L., Forssberg, H., & Ullén, F. (2005). Extensive piano practicing has regionally specific effects on white matter development. *Nature Neuroscience*. https://doi.org/10.1038/nn1516

Buchsbaum, B. R., Greer, S., Chang, W., & Berman, K. F. (2005). Meta‐analysis of neuroimaging studies of the Wisconsin Card‐Sorting task and component processes. *Human Brain Mapping*, *25*(1), 35–45. https://doi.org/10.1002/hbm.20128

Calhoun, V. (2018). Data-driven approaches for identifying links between brain structure and function in health and disease. *Dialogues in Clinical Neuroscience*, *20*(2), 87–99. https://doi.org/10.31887/DCNS.2018.20.2/vcalhoun

Carter, F., Anwander, A., Goucha, T., Adamson, H., Friederici, A. D., Lutti, A., Gauthier, C. J., Weiskopf, N., Bazin, P.-L., & Steele, C. J. (2022). *Assessing Quantitative MRI Techniques using Multimodal Comparisons* (p. 2022.02.10.479780). bioRxiv. https://doi.org/10.1101/2022.02.10.479780

de Lange, A.-M. G., Bråthen, A. C. S., Rohani, D. A., Grydeland, H., Fjell, A. M., & Walhovd, K. B. (2017). The effects of memory training on behavioral and microstructural plasticity in young and older adults. *Human Brain Mapping*, *38*(11), 5666–5680. https://doi.org/10.1002/hbm.23756

Dhollander, T., Raffelt, D., & Connelly, A. (2016, September 11). *Unsupervised 3-tissue response function estimation from single-shell or multi-shell diffusion MR data without a co-registered T1 image*.

Dhollander, T., Raffelt, D., & Connelly, A. (2018). *Accuracy of response function estimation algorithms for 3-tissue spherical deconvolution of diverse quality diffusion MRI data*. International Society for Magnetic Resonance in Medicine (ISMRM).

https://archive.ismrm.org/2018/1569.html

Duval, T., Stikov, N., & Cohen-Adad, J. (2017). Modeling white matter microstructure. *Functional Neurology*, *31*(4), 217–228. https://doi.org/10.11138/FNeur/2016.31.4.217

Figley, C. R., Uddin, M. N., Wong, K., Kornelsen, J., Puig, J., & Figley, T. D. (2022). Potential Pitfalls of Using Fractional Anisotropy, Axial Diffusivity, and Radial Diffusivity as Biomarkers of Cerebral White Matter Microstructure. *Frontiers in Neuroscience*, *15*. https://www.frontiersin.org/articles/10.3389/fnins.2021.799576

Glasser, M. F., Sotiropoulos, S. N., Wilson, J. A., Coalson, T. S., Fischl, B., Andersson, J. L., Xu, J., Jbabdi, S., Webster, M., Polimeni, J. R., Van Essen, D. C., & Jenkinson, M. (2013). The minimal preprocessing pipelines for the Human Connectome Project. *NeuroImage*, *80*, 105–124. https://doi.org/10.1016/j.neuroimage.2013.04.127

Guerrero-Gonzalez, J. M., Yeske, B., Kirk, G. R., Bell, M. J., Ferrazzano, P. A., & Alexander, A. L. (2022). Mahalanobis distance tractometry (MaD-Tract) – a framework for personalized white matter anomaly detection applied to TBI. *NeuroImage*, *260*, 119475. https://doi.org/10.1016/j.neuroimage.2022.119475

Hagmann, P., Sporns, O., Madan, N., Cammoun, L., Pienaar, R., Wedeen, V. J., Meuli, R., Thiran, J.-P., & Grant, P. E. (2010). White matter maturation reshapes structural connectivity in the late developing human brain. *Proceedings of the National Academy of Sciences of the United States of America*, *107*(44), 19067–19072. https://doi.org/10.1073/pnas.1009073107

Hurtubise, J. M., Gorbet, D. J., Hynes, L. M., Macpherson, A. K., & Sergio, L. E. (2020). White Matter Integrity and Its Relationship to Cognitive-Motor Integration in Females with and without Post-Concussion Syndrome. *Journal of Neurotrauma*, *37*(13), 1528–1536.

https://doi.org/10.1089/neu.2019.6765

Jeurissen, B., Tournier, J.-D., Dhollander, T., Connelly, A., & Sijbers, J. (2014). Multi-tissue constrained spherical deconvolution for improved analysis of multi-shell diffusion MRI data. *NeuroImage*, *103*, 411–426. https://doi.org/10.1016/j.neuroimage.2014.07.061

Johansen-Berg, H., Della-Maggiore, V., Behrens, T. E., Smith, S. M., & Paus, T. (2007). Integrity of white matter in the corpus callosum correlates with bimanual co-ordination skills. *NeuroImage*, *36*(Suppl 2), T16–T21. https://doi.org/10.1016/j.neuroimage.2007.03.041

Karnath, H. O., Sperber, C., & Rorden, C. (2018). Mapping human brain lesions and their functional consequences. *NeuroImage*, *165*, 180–189. https://doi.org/10.1016/j.neuroimage.2017.10.028

Knowles, J. K., Batra, A., Xu, H., & Monje, M. (2022). Adaptive and maladaptive myelination in health and disease. *Nature Reviews Neurology*, *18*(12), Article 12. https://doi.org/10.1038/s41582-022-00737-3

Krüger, B., Hettwer, M., Zabicki, A., de Haas, B., Munzert, J., & Zentgraf, K. (2020). Practice modality of motor sequences impacts the neural signature of motor imagery. *Scientific Reports*, *10*, 19176. https://doi.org/10.1038/s41598-020-76214-y

Mahalanobis, P. C. (1936). On the Generalised Distance in Statistics. *Proceedings of the National Institute of Sciences of India*, *2*(1), 49–55.

McIntosh, A. R., & Lobaugh, N. J. (2004). Partial least squares analysis of neuroimaging data: Applications and advances. *NeuroImage*, *23*, S250–S263. https://doi.org/10.1016/j.neuroimage.2004.07.020

McIntosh, A. R., & Mišić, B. (2013). Multivariate Statistical Analyses for Neuroimaging Data. *Annual Review of Psychology*, *64*(1), 499–525.

https://doi.org/10.1146/annurev-psych-113011-143804

McKenzie, I. A., Ohayon, D., Li, H., Paes de Faria, J., Emery, B., Tohyama, K., & Richardson, W. D. (2014). Motor skill learning requires active central myelination. *Science*, *346*(6207), 318–322. https://doi.org/10.1126/science.1254960

Mezer, A., Yeatman, J. D., Stikov, N., Kay, K. N., Cho, N., Dougherty, R. F., Perry, M. L., Parvizi, J., Hua, L. H., Butts-Pauly, K., & Wandell, B. (2013). Quantifying the local tissue volume and composition in individual brains with MRI. *Nature Medicine*, *19*(12), 1667–1672. https://doi.org/10.1038/nm.3390

Muetzel, R. L., Collins, P. F., Mueller, B. A., M. Schissel, A., Lim, K. O., & Luciana, M. (2008). The development of corpus callosum microstructure and associations with bimanual task performance in healthy adolescents. *NeuroImage*, *39*(4), 1918–1925. https://doi.org/10.1016/j.neuroimage.2007.10.018

Owen, T. W., de Tisi, J., Vos, S. B., Winston, G. P., Duncan, J. S., Wang, Y., & Taylor, P. N. (2021). Multivariate white matter alterations are associated with epilepsy duration. *The European Journal of Neuroscience*, *53*(8), 2788–2803. https://doi.org/10.1111/ejn.15055

Pajevic, S., Basser, P. J., & Fields, R. D. (2014). Role of Myelin Plasticity in Oscillations and Synchrony of Neuronal Activity. *Neuroscience*, *276*, 135–147. https://doi.org/10.1016/j.neuroscience.2013.11.007

Pan, S., Mayoral, S. R., Choi, H. S., Chan, J. R., & Kheirbek, M. A. (2020). Preservation of a remote fear memory requires new myelin formation. *Nature Neuroscience*, *23*(4), 487–499. https://doi.org/10.1038/s41593-019-0582-1

Penny, K. I. (1996). Appropriate Critical Values When Testing for a Single Multivariate Outlier by Using the Mahalanobis Distance. *Journal of the Royal Statistical Society Series C:*

Applied Statistics, *45*(1), 73–81. https://doi.org/10.2307/2986224

Poldrack, R. A. (2010). Mapping mental function to brain structure: How can cognitive neuroimaging succeed? *Perspectives on Psychological Science : A Journal of the Association for Psychological Science*, *5*(5), 753–761. https://doi.org/10.1177/1745691610388777

Price, C. J., & Friston, K. J. (2005). Functional ontologies for cognition: The systematic definition of structure and function. *Cognitive Neuropsychology*, *22*(3–4), 262–275. https://doi.org/10.1080/02643290442000095

Pur, D. R., Preti, M. G., de Ribaupierre, A., Van De Ville, D., Eagleson, R., Mella, N., & de Ribaupierre, S. (2022). Mapping of Structure-Function Age-Related Connectivity Changes on Cognition Using Multimodal MRI. *Frontiers in Aging Neuroscience*, *14*, 757861. https://doi.org/10.3389/fnagi.2022.757861

Raffelt, D. A., Smith, R. E., Ridgway, G. R., Tournier, J.-D., Vaughan, D. N., Rose, S., Henderson, R., & Connelly, A. (2015). Connectivity-based fixel enhancement: Whole-brain statistical analysis of diffusion MRI measures in the presence of crossing fibres. *Neuroimage*, *117*, 40–55. https://doi.org/10.1016/j.neuroimage.2015.05.039

Raffelt, D. A., Tournier, J.-D., Smith, R. E., Vaughan, D. N., Jackson, G., Ridgway, G. R., & Connelly, A. (2017). Investigating white matter fibre density and morphology using fixel-based analysis. *NeuroImage*, *144*, 58–73. https://doi.org/10.1016/j.neuroimage.2016.09.029

Raffelt, D., Tournier, J.-D., Rose, S., Ridgway, G. R., Henderson, R., Crozier, S., Salvado, O., & Connelly, A. (2012). Apparent Fibre Density: A novel measure for the analysis of diffusion-weighted magnetic resonance images. *NeuroImage*, *59*(4), 3976–3994.

https://doi.org/10.1016/j.neuroimage.2011.10.045

Raghavan, S., Reid, R. I., Przybelski, S. A., Lesnick, T. G., Graff-Radford, J., Schwarz, C. G., Knopman, D. S., Mielke, M. M., Machulda, M. M., Petersen, R. C., Jack, C. R., & Vemuri, P. (2021). Diffusion models reveal white matter microstructural changes with ageing, pathology and cognition. *Brain Communications*, *3*(2), fcab106. https://doi.org/10.1093/braincomms/fcab106

Reuben, D. B., Magasi, S., McCreath, H. E., Bohannon, R. W., Wang, Y. C., Bubela, D. J., Rymer, W. Z., Beaumont, J., Rine, R. M., Lai, J. S., & Gershon, R. C. (2013). Motor assessment using the NIH Toolbox. *Neurology*, *80*(11 Suppl 3), S65–S65. https://doi.org/10.1212/wnl.0b013e3182872e01

Rodríguez-Aranda, C., Mittner, M., & Vasylenko, O. (2016). Association Between Executive Functions, Working Memory, and Manual Dexterity in Young and Healthy Older Adults: An Exploratory Study. *Perceptual and Motor Skills*, *122*(1), 165–192. https://doi.org/10.1177/0031512516628370

Rolls, E. T., Joliot, M., & Tzourio-Mazoyer, N. (2015). Implementation of a new parcellation of the orbitofrontal cortex in the automated anatomical labeling atlas. *NeuroImage*, *122*, 1–5. https://doi.org/10.1016/j.neuroimage.2015.07.075

Sampaio-Baptista, C., Khrapitchev, A. A., Foxley, S., Schlagheck, T., Scholz, J., Jbabdi, S., DeLuca, G. C., Miller, K. L., Taylor, A. E., Thomas, N., Kleim, J. A., Sibson, N. R., Bannerman, D. M., & Johansen-Berg, H. (2013). Motor Skill Learning Induces Changes in White Matter Microstructure and Myelination. *The Journal of Neuroscience*, *33*(50), 19499–19503. https://doi.org/10.1523/jneurosci.3048-13.2013

Scholz, J., Klein, M. C., Behrens, T. E. J., & Johansen-Berg, H. (2009). Training induces changes

in white-matter architecture. *Nature Neuroscience*, *12*(11), 1370–1371. https://doi.org/10.1038/nn.2412

Schöttner, M., Bolton, T. A. W., Patel, J., Nahálka, A. T., Vieira, S., & Hagmann, P. (2023). Exploring the latent structure of behavior using the Human Connectome Project's data. *Scientific Reports*, *13*(1), Article 1. https://doi.org/10.1038/s41598-022-27101-1

Seidler, R. D., Bo, J., & Anguera, J. A. (2012). Neurocognitive Contributions to Motor Skill Learning: The Role of Working Memory. *Journal of Motor Behavior*, *44*(6), 445–453. https://doi.org/10.1080/00222895.2012.672348

Sergio, L. E., Gorbet, D. J., Adams, M. S., & Dobney, D. M. (2020). The Effects of Mild Traumatic Brain Injury on Cognitive-Motor Integration for Skilled Performance. *Frontiers in Neurology*, *11*. https://www.frontiersin.org/articles/10.3389/fneur.2020.541630

Smith, R. E., Tournier, J.-D., Calamante, F., & Connelly, A. (2012). Anatomically-constrained tractography: Improved diffusion MRI streamlines tractography through effective use of anatomical information. *NeuroImage*, *62*(3), 1924–1938. https://doi.org/10.1016/j.neuroimage.2012.06.005

Soares, J., Marques, P., Alves, V., & Sousa, N. (2013). A hitchhiker's guide to diffusion tensor imaging. *Frontiers in Neuroscience*. http://dx.doi.org/10.3389/fnins.2013.00031

Sobinov, A. R., & Bensmaia, S. J. (2021). The neural mechanisms of manual dexterity. *Nature Reviews. Neuroscience*, *22*(12), 741–757. https://doi.org/10.1038/s41583-021-00528-7

Steele, C. J., Bailey, J. A., Zatorre, R. J., & Penhune, V. B. (2013). Early musical training and white-matter plasticity in the corpus callosum: Evidence for a sensitive period. *Journal of Neuroscience*, *33*(3), 1282–1290. https://doi.org/10.1523/JNEUROSCI.3578-12.2013

Stikov, N., Campbell, J. S. W., Stroh, T., Lavelée, M., Frey, S., Novek, J., Nuara, S., Ho, M.-K., Bedell, B. J., Dougherty, R. F., Leppert, I. R., Boudreau, M., Narayanan, S., Duval, T., Cohen-Adad, J., Picard, P.-A., Gasecka, A., Côté, D., & Pike, G. B. (2015). In vivo histology of the myelin g-ratio with magnetic resonance imaging. *NeuroImage*, *118*, 397–405. https://doi.org/10.1016/j.neuroimage.2015.05.023

Suchan, B., Yágüez, L., Wunderlich, G., Canavan, A. G. M., Herzog, H., Tellmann, L., Hömberg, V., & Seitz, R. J. (2002). Neural correlates of visuospatial imagery. *Behavioural Brain Research*, *131*(1–2), 163–168. https://doi.org/10.1016/S0166-4328(01)00373-4

Talozzi, L., Forkel, S. J., Pacella, V., Nozais, V., Allart, E., Piscicelli, C., Pérennou, D., Tranel, D., Boes, A., Corbetta, M., Nachev, P., & Thiebaut de Schotten, M. (2023). Latent disconnectome prediction of long-term cognitive-behavioural symptoms in stroke. *Brain*, *146*(5), 1963–1978. https://doi.org/10.1093/brain/awad013

Tardif, C. L., Gauthier, C. J., Steele, C. J., Bazin, P.-L., Schäfer, A., Schaefer, A., Turner, R., & Villringer, A. (2016). Advanced MRI techniques to improve our understanding of experience-induced neuroplasticity. *NeuroImage*, *131*, 55–72. https://doi.org/10.1016/j.neuroimage.2015.08.047

Taubert, M., Draganski, B., Anwander, A., Müller, K., Horstmann, A., Villringer, A., & Ragert, P. (2010). Dynamic properties of human brain structure: Learning-related changes in cortical areas and associated fiber connections. *The Journal of Neuroscience: The Official Journal of the Society for Neuroscience*, *30*(35), 11670–11677. https://doi.org/10.1523/JNEUROSCI.2567-10.2010

Taylor, P. N., Silva, N. M. da, Blamire, A., Wang, Y., & Forsyth, R. (2020). Early deviation from

normal structural connectivity: A novel intrinsic severity score for mild TBI. *Neurology*, *94*(10), e1021–e1026. https://doi.org/10.1212/WNL.0000000000008902

Thiebaut de Schotten, M., & Forkel, S. J. (2022). The emergent properties of the connected brain. *Science*, *378*(6619), 505–510. https://doi.org/10.1126/science.abq2591

Thiebaut de Schotten, M., Foulon, C., & Nachev, P. (2020). Brain disconnections link structural connectivity with function and behaviour. *Nature Communications*, *11*, 5094. https://doi.org/10.1038/s41467-020-18920-9

Tournier, J.-D., Smith, R., Raffelt, D., Tabbara, R., Dhollander, T., Pietsch, M., Christiaens, D., Jeurissen, B., Yeh, C.-H., & Connelly, A. (2019). MRtrix3: A fast, flexible and open software framework for medical image processing and visualisation. *NeuroImage*, *202*, 116137. https://doi.org/10.1016/j.neuroimage.2019.116137

Tremblay, S. A., Alasmar, Z., Pirhadi, A., Carbonell, F., Iturria-Medina, Y., Gauthier, C. J., & Steele, C. J. (2024). MVComp toolbox: MultiVariate Comparisons of brain MRI features accounting for common information across measures. *Aperture Neuro*, *4*. https://doi.org/10.52294/001c.118427

Tremblay, S. A., Jäger, A.-T., Huck, J., Giacosa, C., Beram, S., Schneider, U., Grahl, S., Villringer, A., Tardif, C. L., Bazin, P.-L., Steele, C. J., & Gauthier, C. J. (2021). White matter microstructural changes in short-term learning of a continuous visuomotor sequence. *Brain Structure & Function*, *226*(6), 1677–1698. https://doi.org/10.1007/s00429-021-02267-y

Tustison, N. J., Avants, B. B., Cook, P. A., Zheng, Y., Egan, A., Yushkevich, P. A., & Gee, J. C. (2010). N4ITK: Improved N3 Bias Correction. *IEEE Transactions on Medical Imaging*, *29*(6), 1310–1320. https://doi.org/10.1109/TMI.2010.2046908

Uddin, Md. N., Figley, T. D., Solar, K. G., Shatil, A. S., & Figley, C. R. (2019). Comparisons between multi-component myelin water fraction, T1w/T2w ratio, and diffusion tensor imaging measures in healthy human brain structures. *Scientific Reports*, *9*, 2500. https://doi.org/10.1038/s41598-019-39199-x

Van Essen, D. C., Smith, S. M., Barch, D. M., Behrens, T. E. J., Yacoub, E., & Ugurbil, K. (2013). The WU-Minn Human Connectome Project: An overview. *NeuroImage*, *80*, 62–79. https://doi.org/10.1016/j.neuroimage.2013.05.041

Varoquaux, G., & Poldrack, R. A. (2019). Predictive models avoid excessive reductionism in cognitive neuroimaging. *Current Opinion in Neurobiology*, *55*, 1–6. https://doi.org/10.1016/j.conb.2018.11.002

Varoquaux, G., Schwartz, Y., Poldrack, R. A., Gauthier, B., Bzdok, D., Poline, J.-B., & Thirion, B. (2018). Atlases of cognition with large-scale human brain mapping. *PLOS Computational Biology*, *14*(11), e1006565. https://doi.org/10.1371/journal.pcbi.1006565

Voigt, K., Liang, E. X., Misic, B., Ward, P. G. D., Egan, G. F., & Jamadar, S. D. (2023). Metabolic and functional connectivity provide unique and complementary insights into cognition-connectome relationships. *Cerebral Cortex (New York, N.Y.: 1991)*, *33*(4), 1476–1488. https://doi.org/10.1093/cercor/bhac150

Weber, K. A., Teplin, Z. M., Wager, T. D., Law, C. S. W., Prabhakar, N. K., Ashar, Y. K., Gilam, G., Banerjee, S., Delp, S. L., Glover, G. H., Hastie, T. J., & Mackey, S. (2022). Confounds in neuroimaging: A clear case of sex as a confound in brain-based prediction. *Frontiers in Neurology*, *13*, 960760. https://doi.org/10.3389/fneur.2022.960760

Weintraub, S., Dikmen, S. S., Heaton, R. K., Tulsky, D. S., Zelazo, P. D., Bauer, P. J., Carlozzi, N. E., Slotkin, J., Blitz, D., Wallner-Allen, K., Fox, N. A., Beaumont, J. L., Mungas, D.,

Nowinski, C. J., Richler, J., Deocampo, J. A., Anderson, J. E., Manly, J. J., Borosh, B., … Gershon, R. C. (2013). Cognition assessment using the NIH Toolbox. *Neurology*, *80*(11 Suppl 3), S54. https://doi.org/10.1212/WNL.0b013e3182872ded

Yoo, K., Rosenberg, M. D., Noble, S., Scheinost, D., Constable, R. T., & Chun, M. M. (2019). Multivariate approaches improve the reliability and validity of functional connectivity and prediction of individual behaviors. *NeuroImage*, *197*, 212–223. https://doi.org/10.1016/j.neuroimage.2019.04.060

Zayed, A., Iturria-Medina, Y., Villringer, A., Sehm, B., & Steele, C. J. (2020). Rapid Quantification of White Matter Disconnection in the Human Brain. *2020 42nd Annual International Conference of the IEEE Engineering in Medicine & Biology Society (EMBC)*, 1701–1704. https://doi.org/10.1109/EMBC44109.2020.9176229

Zhang, H., Schneider, T., Wheeler-Kingshott, C. A., & Alexander, D. C. (2012). NODDI: Practical in vivo neurite orientation dispersion and density imaging of the human brain. *NeuroImage*, *61*(4), 1000–1016. https://doi.org/10.1016/j.neuroimage.2012.03.072

Ziegler, G., Dahnke, R., Winkler, A. D., & Gaser, C. (2013). Partial least squares correlation of multivariate cognitive abilities and local brain structure in children and adolescents. *NeuroImage*, *82*, 284–294. https://doi.org/10.1016/j.neuroimage.2013.05.088

7. Appendix A

Supplementary figure 1: the association between each task and D2 scores at each voxel.

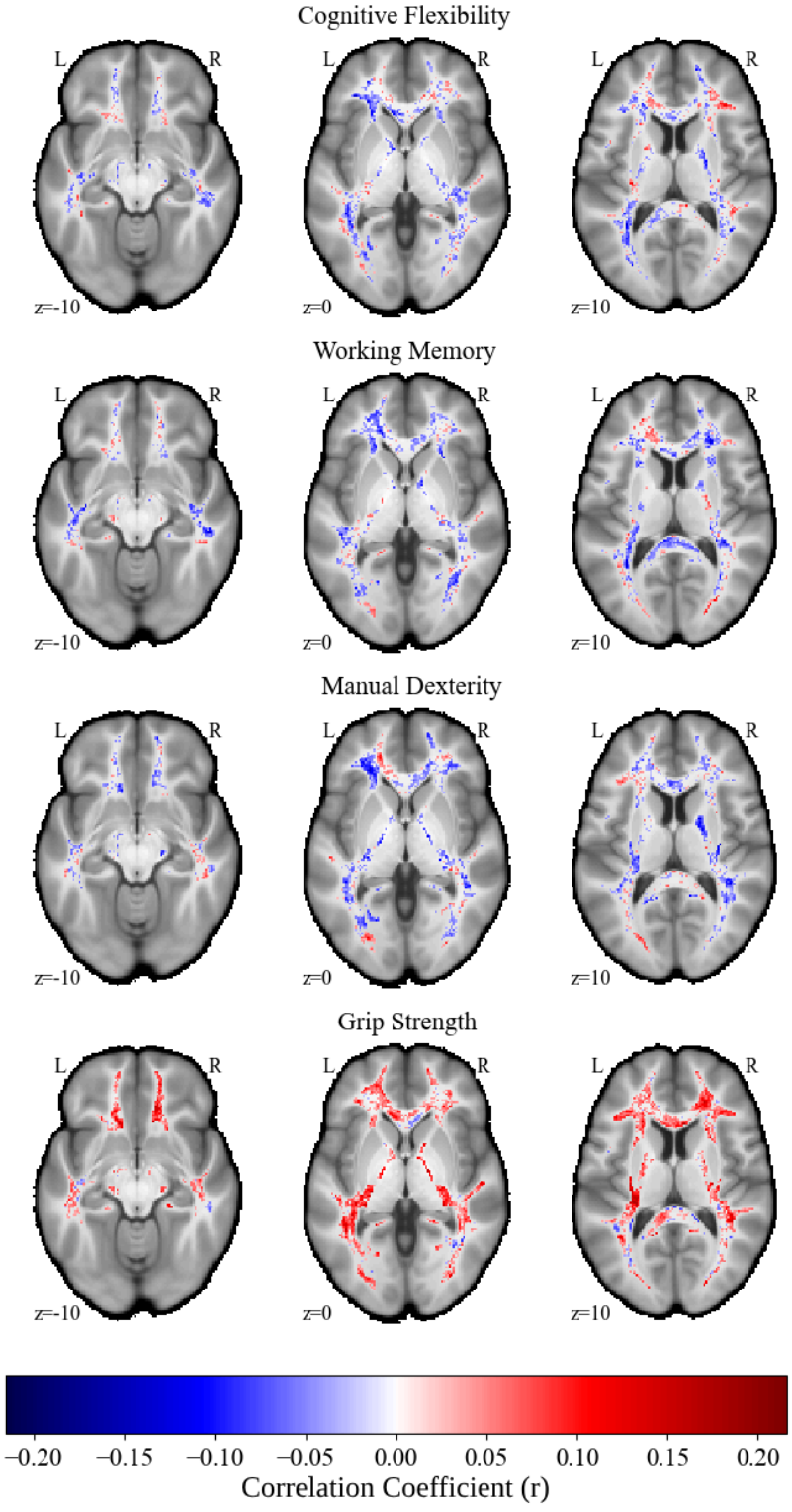

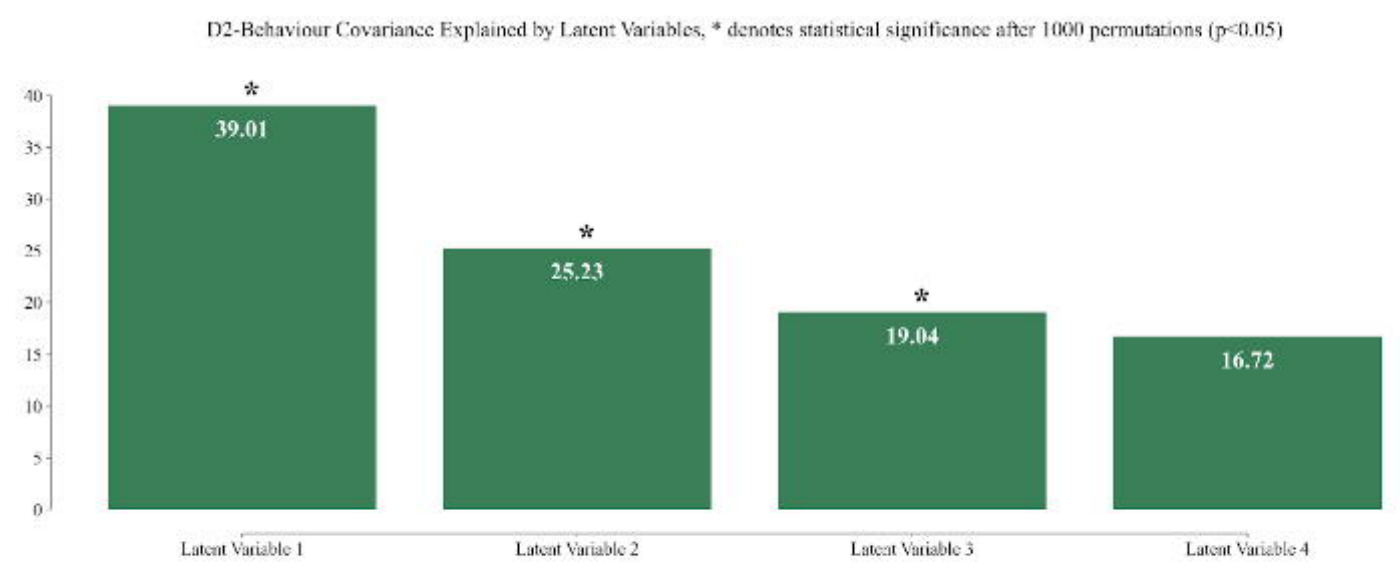

Figure 1: The amount of explained brain-behaviour covariance per latent variable. * denotes statistically significant after 1000 permutations (FWE $p < 0.05$).

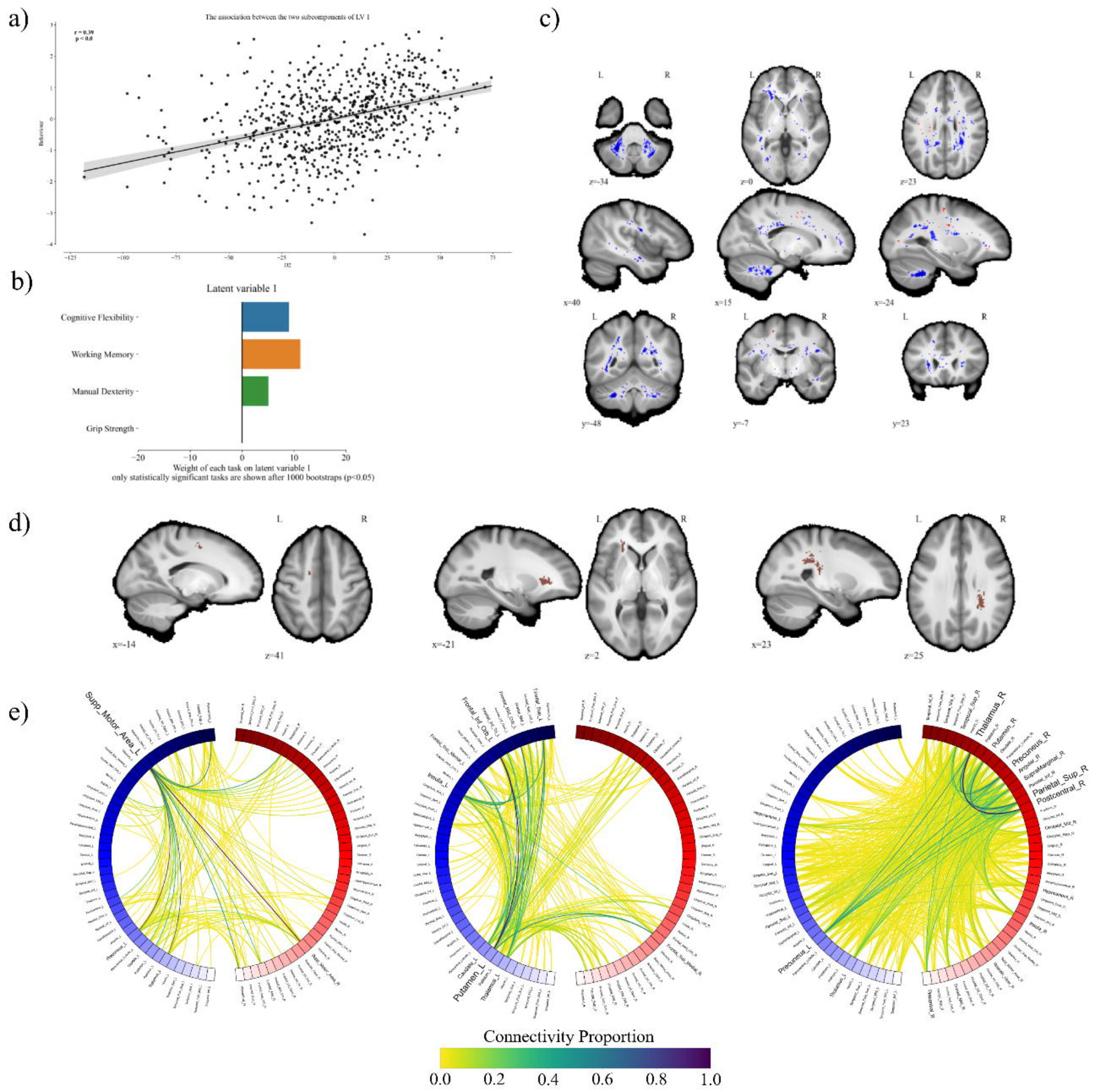
a)
The association between the two subcomponents of LV 1
r = 0.39
p < 0.0
Behaviour
DI2
b)
Latent variable 1
Cognitive Flexibility
Working Memory
Manual Dexterity
Grip Strength
Weight of each task on latent variable 1
only statistically significant tasks are shown after 1000 bootstraps (p<0.05)
c)
L
R
z=-34
z=0
z=23
x=40
x=15
x=-24
y=-48
y=-7
y=23
d)
x=-14
z=41
x=-21
z=2
x=23
z=25
e)
Supp_Motor_Area_L
Frontal_Inf_Orb_L
Insula_L
Caudate_L
Putamen_L
Thalamus_L
Thalamus_R
Putamen_R
Precuneus_R
Angular_R
SupraMarginal_R
Parietal_Sup_R
Postcentral_R
Precuneus_L
Connectivity Proportion
0.0
0.2
0.4
0.6
0.8
1.0

a)

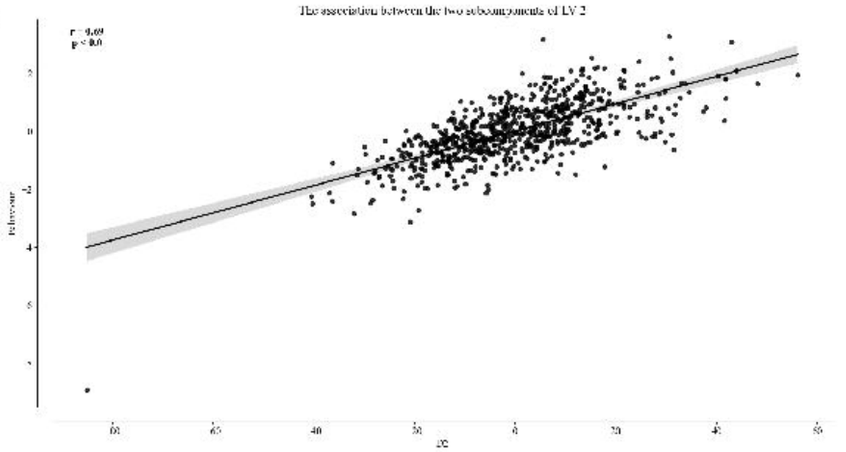
The association between the two subcomponents of LV 2

b)

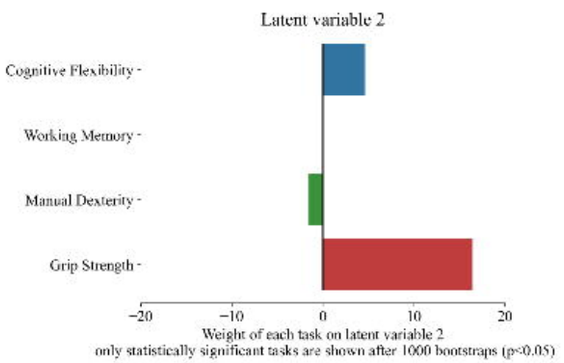
Latent variable 2
Cognitive Flexibility
Working Memory
Manual Dexterity
Grip Strength
−20
−10
0
10
20
Weight of each task on latent variable 2
only statistically significant tasks are shown after 1000 bootstraps (p<0.05)

c)

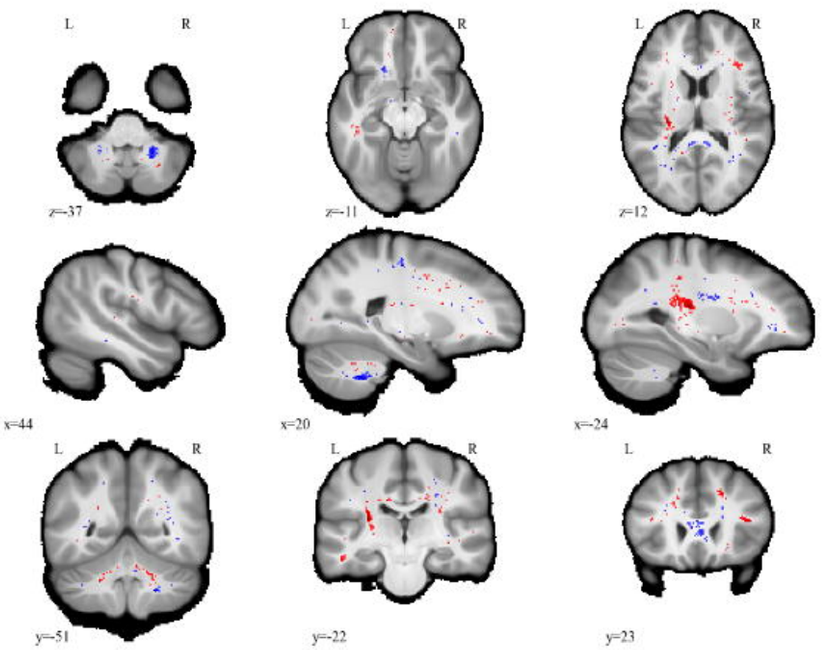
L
R
z=-37
z=-11
z=12
x=44
x=20
x=-24
y=-51
y=-22
y=23

d)

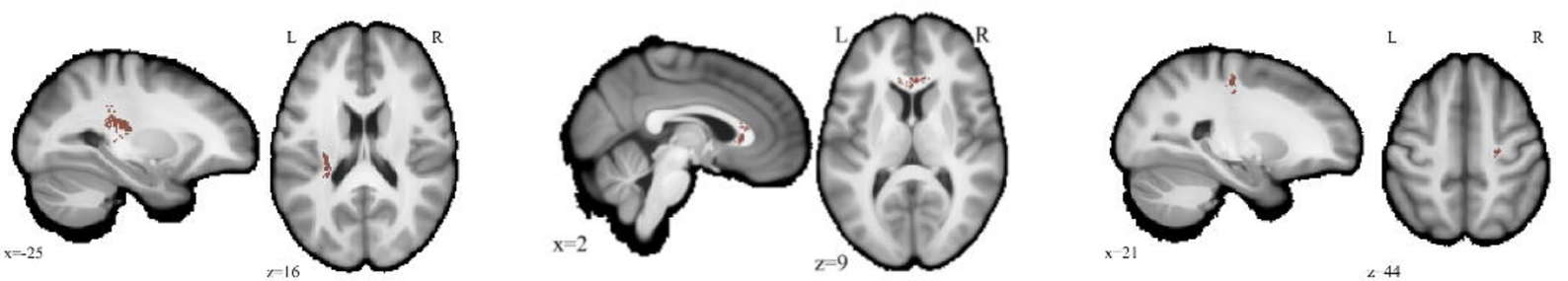
L
R
x=-25
z=16
x=2
z=9
x=21
z=44

e)

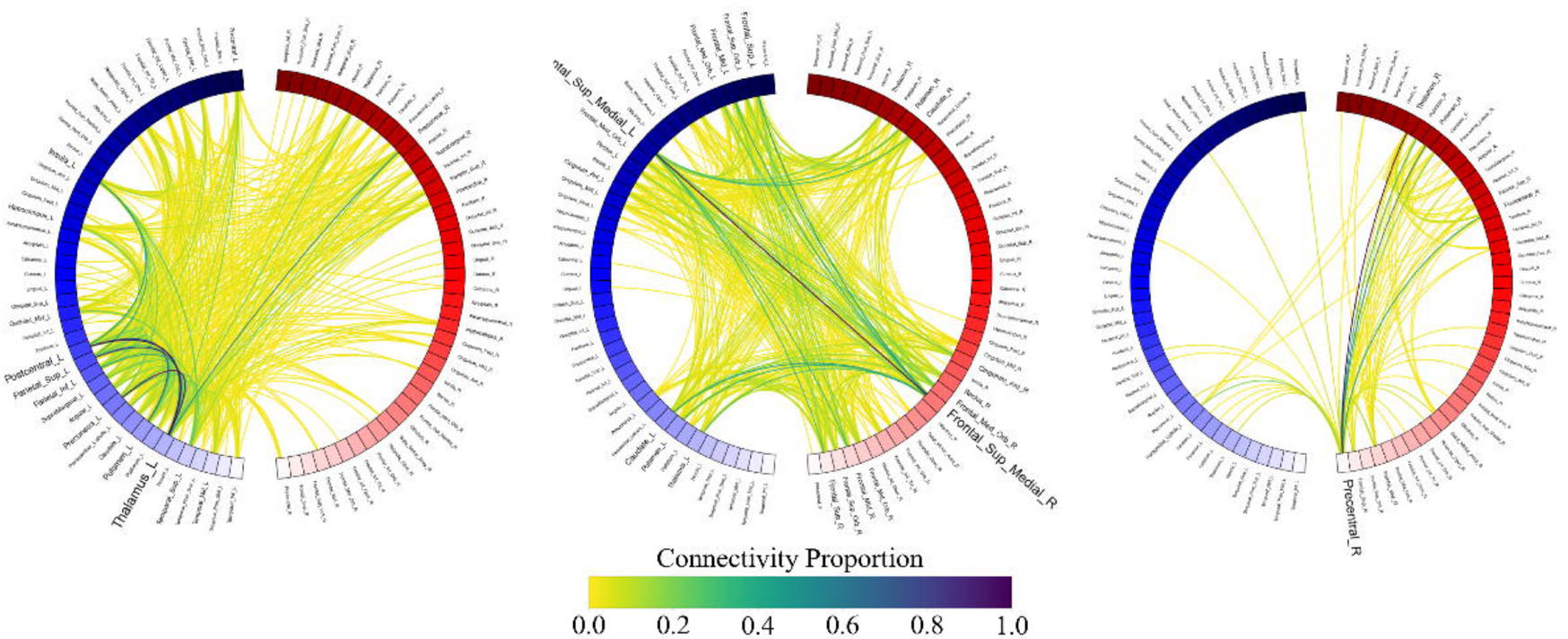
Thalamus_L
Postcentral_L
Parietal_Sup_L
Frontal_Inf_L
Insula_L
Frontal_Sup_Medial_L
Frontal_Sup_Medial_R
Frontal_Med_Orb_R
Precentral_R
Connectivity Proportion
0.0
0.2
0.4
0.6
0.8
1.0

a)

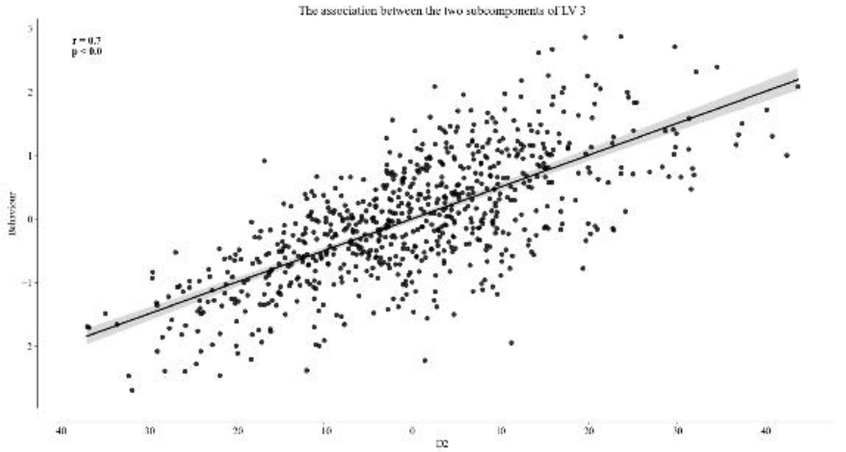
The association between the two subcomponents of LV 3
r = 0.7
p < 0.0
Behrvior
DC

b)

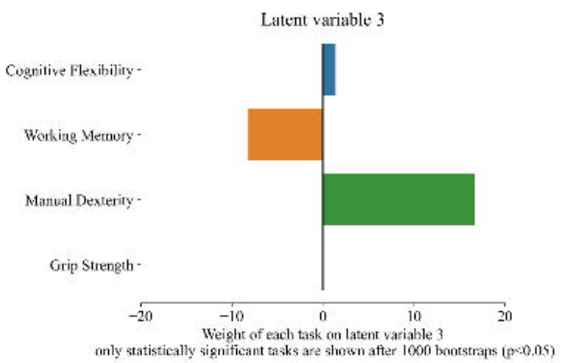
Latent variable 3
Cognitive Flexibility
Working Memory
Manual Dexterity
Grip Strength
−20
−10
0
10
20
Weight of each task on latent variable 3
only statistically significant tasks are shown after 1000 bootstraps (p<0.05)

c)

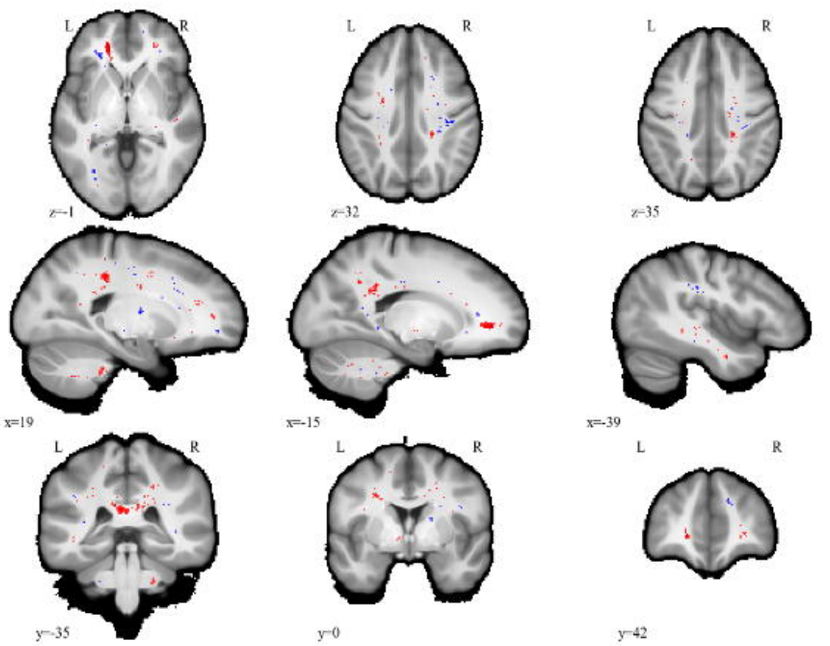
L
R
z=-1
z=32
z=35
x=19
x=-15
x=-39
y=-35
y=0
y=42

d)

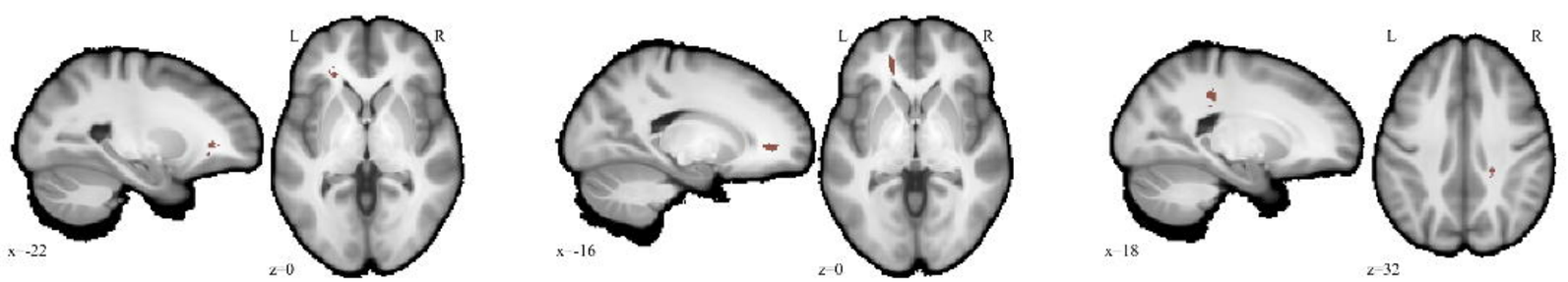
L
R
x=-22
z=0
x=-16
z=0
x=18
z=32

e)

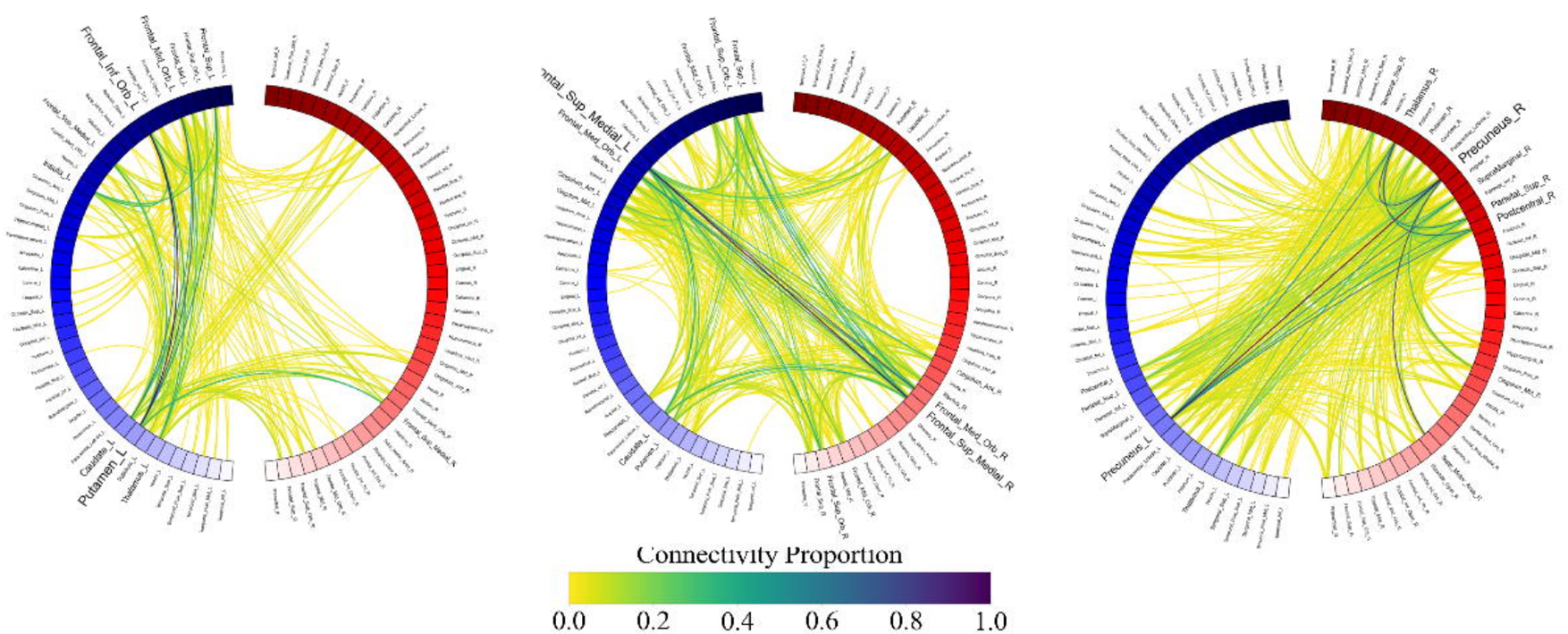
Frontal_Inf_Orb_L
Putamen_L
Frontal_Sup_Medial_L
Frontal_Med_Orb_R
Frontal_Sup_Medial_R
Precuneus_R
Precuneus_L
Connectivity Proportion
0.0
0.2
0.4
0.6
0.8
1.0